

**Weather-Driven Power System Operations: Integrating  
Machine Learning, Resilience Forecasting, and Grid  
Optimization for Climate Adaptation**

by

**Jasmine Danielle Garland**

B.Sc., Appalachian State University, 2020

M.Sc., University of Colorado Boulder, 2023

A thesis submitted to the  
Faculty of the Graduate School of the  
University of Colorado in partial fulfillment  
of the requirements for the degree of  
Doctor of Philosophy

Department of Civil, Environmental, and Architectural Engineering

2025

Committee Members:

Kyri Baker, Chair

Ben Livneh

Thora Nea

Garland, Jasmine Danielle (Ph.D., Architectural Engineering)

Weather-Driven Power System Operations: Integrating Machine Learning, Resilience Forecasting,  
and Grid Optimization for Climate Adaptation

Thesis directed by Prof. Kyri Baker

Often the abstract will be long enough to require more than one page, in which case the macro “\OnePageChapter” should *not* be used.

But this one isn’t, so it should.

## Contents

### Chapter

<b>1</b>	<b>Introduction</b>	<b>1</b>
1.1	Motivation . . . . .	1
1.2	Research Questions . . . . .	1
1.3	Expected Outcomes . . . . .	2
<b>2</b>	<b>For the Reader: An Introduction to Weather Driven Power Systems</b>	<b>3</b>
2.1	Overview of Climate Modeling . . . . .	3
2.1.1	Emission Scenarios . . . . .	4
2.1.2	Risk-Based Approaches . . . . .	5
2.1.3	Regional Climate Models . . . . .	6
2.1.4	Power Sector Modeling . . . . .	6
2.2	Extreme Weather Events . . . . .	7
2.2.1	Heatwaves . . . . .	8
2.2.2	Extreme Cold Temperatures . . . . .	9
2.2.3	Droughts . . . . .	9
2.2.4	Non-Hurricane and Non-Tornadic Winds . . . . .	10
2.2.5	Wildfires . . . . .	10
2.2.6	Adaptation . . . . .	10

<b>3 For Frontline Communities: Energy Burden and Social Vulnerability in the Energy Transition</b>	<b>14</b>
<b>3.1 Background</b>	<b>14</b>
<b>3.2 Study Regions and Data Explanation</b>	<b>15</b>
<b>3.3 Unsupervised Learning for Energy Policy Design: Insights from Self-Organizing Maps</b>	<b>18</b>
<b>3.3.1 Methods</b>	<b>18</b>
<b>3.3.2 Results</b>	<b>20</b>
<b>3.4 Exploring the importance of Environmental Justice variables for predicting Energy Burden in the Contiguous United States</b>	<b>20</b>
<b>3.4.1 Methods</b>	<b>20</b>
<b>3.4.2 Results</b>	<b>22</b>
<b>3.5 Discussion</b>	<b>32</b>
<b>4 For Proactive Grid Management: Forecasting Weather-Driven Power Outages and Duration</b>	<b>35</b>
<b>4.1 Introduction</b>	<b>35</b>
<b>4.2 Learning to Predict Power Outage Durations from Historical Weather Data: Comparing Machine Learning Models</b>	<b>36</b>
<b>4.2.1 Study Region and Data</b>	<b>36</b>
<b>4.2.2 Methods</b>	<b>36</b>
<b>4.2.2.1 Results</b>	<b>38</b>
<b>4.2.2.2 Power Outage Duration Prediction (Regression)</b>	<b>38</b>
<b>4.2.2.3 Power Outage Occurrence Prediction (Classification)</b>	<b>42</b>
<b>4.2.2.4 Reliability Metrics</b>	<b>44</b>
<b>4.2.3 Weather-Aware Predictions for Power Disruptions and Forecasting</b>	<b>45</b>
<b>4.2.3.1 Study Region and Data</b>	<b>45</b>
<b>4.2.3.2 Methods</b>	<b>46</b>
<b>4.2.3.3 Variable Importance</b>	<b>51</b>

4.4.4 Implementation Example . . . . .	52
4.5 Conclusion . . . . .	52
<b>5 For Power Grid Operations: Carbon-Aware Operational Strategy Evaluation</b>	<b>55</b>
5.1 Test Cases and Grid Topologies . . . . .	56
5.1.1 IEEE 118-Bus Test Case . . . . .	56
5.1.2 United Kingdom . . . . .	56
5.1.3 Electric Reliability Council of Texas . . . . .	56
5.2 Dispatch Methods . . . . .	56
5.3 Preliminary Results . . . . .	58
<b>6 For Power System Planning in Colorado: Adapting Capacity Expansion to Climate Change and Solar Growth</b>	<b>60</b>
6.1 Test Case . . . . .	60
6.2 Methods . . . . .	60
6.3 Simulation Evaluation . . . . .	60
<b>7 Future Work</b>	<b>61</b>
7.1 For Power System Planning in Switzerland: Capacity Expansion under Climate Stress	61
7.2 For Power System Modelers: Evaluating Topology and Dispatch Strategies with Realistic and Simplified Grid Models . . . . .	61
7.3 Research Plan . . . . .	61
<b>Bibliography</b>	<b>62</b>
<b>Appendix</b>	
<b>A Weird Exam Answers</b>	<b>70</b>



## Tables

### **Table**

<b>2.1 Emission Scenario Categories From the IPCC</b>	
This table presents Emission Scenarios from the IPCC fourth, fifth, and sixth reports. A.R.	
represents the IPCC Annual Report, paired with RCP for AR5 and AR6. Prior to RCPs,	
SRES were used in AR4. . . . .	5
<b>2.2 Common Power System Hardening Measures [38, 76]</b>	
System hardening improves system infrastructure durability and stability, improving re-	
silience and reliability through the lens of weather-related activity. System hardening is	
especially useful in existing power infrastructure. The measures provided are commonly	
implemented system hardening techniques. . . . .	11
<b>2.3 Summarization of Adaptation Measures and Knowledge Gaps</b>	
A summary of power system adaptation measures suggested for the future and knowledge	
gaps suggested for future studies. . . . .	12
<b>3.1 Energy Burden Data Overview</b>	
T . . . . .	17
<b>3.2 Energy Burden Results Summary</b>	
A summary of the SOM results for each census region. . . . .	20
<b>3.3 Exhaustive Search Subset Selection Methods</b>	
The indicators selected for each region from the exhaustive search subset selection using all	
data values. . . . .	25

### **3.4 Principle Component Analysis Magnitude**

For each region, the data groups are shown with their respective magnitude of influence within the first three PCs. The building characteristics, followed by the environmental justice variables, consistently show the most significant magnitude of influence within the first PC, which is the PC that explains the highest level of data variance. . . . . 25

### **3.5 Energy Burden Full Indicator Set Best Models**

The model with the highest  $R^2$  value for each region and modeling framework using the full indicator set. The region, modeling method, and the indicators used are shown, with the corresponding  $R^2$ , RMSE, and MAE values. In terms of  $R^2$  the GAMs outperform the random forests in all regions except for the West region, which has the same  $R^2$  value. Regarding the MAE and RMSE, the best performing models show mixed results among the GAMs and random forests. Given the different modeling methods, indicators used, and regions, this table should not be used as a direct comparison. . . . . 28

### **3.6 Energy Burden Principal Component Analysis Best Models**

The model with the highest  $R^2$  value for each region and modeling framework using the PCs. The region, modeling method, and the indicators used are shown, with the corresponding  $R^2$ , RMSE, and MAE values. For PCs, the GAMs outperformed the random forests for each of the modeling metrics. . . . . 29

<b>4.1 Regression and Classification Models Evaluated</b>	. . . . .	36
<b>4.2 Hyperparameter Selection – California Date-Time Split</b>	. . . . .	41
<b>4.3 Hyperparameter Selection – Los Angeles County Date-Time Split</b>	. . . . .	41
<b>4.4 Hyperparameter Selection – Alpine County Date-Time Split</b>	. . . . .	42
<b>4.5 State of California Outage Occurrence Hyper-Parameters</b>	. . . . .	43
<b>4.6 Los Angeles County Outage Occurrence Hyper-Parameters</b>	. . . . .	43
<b>4.7 Alpine County Power Outage Occurrence Hyper-Parameters</b>	. . . . .	44
<b>4.8 SAIDI Calculation for Test and Predicted Outage Durations</b>	. . . . .	44

4.9 CAIFI Calculation for Test and Predicted Outage Occurrence . . . . .	45
4.10 Model Inputs: Meteorological Variables . . . . .	46
4.11 Hyperparameters Trained on 12-Hour Lead Times . . . . .	48
4.12 Performance Metrics for Best Models by Region and Lead Time . . . . .	50

Figures

## Figure

<b>2.1 U.S. Natural Disaster Occurrence and Cost since 1980</b>	
The cost data is represented by the solid bars in USD and is Consumer Price Index adjusted.	
The event occurrences are presented by dashed lines for each year. Both cost and occurrence	
data are provided by [72]. A consistent increase in wildfire costs has been present since 2017.	
Tropical cyclone occurrence and cost do not correlate, while events such as drought and flood	
most commonly alternate over the years. . . . .	8
<b>2.2 Duration of Major Power Outages in the CONUS</b>	
The power outage duration in hours shown per weather event for power outages impacting	
500,000 customers or more between 2000-2021 [1]. . . . .	9
<b>3.1 County Level Energy Burden per Census Region</b>	
The county level energy burden in each census region: west, midwest, south, and northeast.	
States outlined in green are the west region, states outlined in blue are the midwest region,	
states outlined in red are the south region, and states outlined in orange are the northeast	
region. An energy burden of 6% or higher is considered a high energy burden. . . . .	16
<b>3.2 The Self-Organizing Map Process</b>	
The five key step in the SOM process . . . . .	18
<b>3.3 Unsupervised Learning Methods</b>	
The process begins with identifying the input data (red), then the SOMs are completed	
(pink), followed but the post-processing (blue). . . . .	19

<b>3.4 SOM Node Selection per Census Region</b>	
Each census region is shown at the county level, and the counties are categorized by the SOM node they were assigned to. The west and northeast both used a 3x4 topology, and the south used a 4x3, thus each of these regions have 12 nodes. The midwest used a 4x4 SOM topology and has 16 nodes.	21
<b>3.5 Distribution of Select Energy Burden Indicators</b>	21
<b>3.6 Methodology Framework</b>	
A brief description of the processes taken for each modeling framework. The pink represents processes applied to both modeling frameworks, while the blue is specific to framework one and the green is specific to framework two. Overall, two datasets, the full indicator set, and the principle components, are subjected to an exhaustive subset selection search. Then, 3,003 data sets are created from all combinations of 5 indicators. The data sets are then used in the GAM framework and random forest framework.	23
<b>3.7 Modeling Method Variable Selection for the Top 100 Models</b>	
The variables that appeared in the top 100 models for each region using the full indicator set. Each region is assigned a color, while the bar width depends on the number of regions that include the variable. Each variable is given the same spatial width, but the individual bar size depends on the regions included.	26

3.8 Leave-One-Column-Out Analysis Indicator Influence for the West Region	
a) Represents the LOCO analysis for the GAM full indicator set in the South region	b)
Represents the LOCO analysis for the random forest full indicator set in the South region	
c) Represents the LOCO analysis for the GAM PCs in the South region	d) Represents the
LOCO analysis for the random forest PCs in the South region. Each indicator in the top	
100 models for the GAMs and the random forest is subjected to a LOCO analysis. Here,	
the $R^2$ value is provided for the entire model, meaning all the indicators for that model were	
included (red), and the LOCO model, meaning that one indicator was left out of the model	
(blue). The indicator dropped in the LOCO model is provided by the x-axis, and the change	
in $R^2$ is presented on the y-axis. Poverty status, population, and low-income individuals	
have the most significant impact on the $R^2$ value in both the GAMs and random forests for	
the full indicator set. Regarding the PCs, the first PC has the most significant effect on	
model performance for both the GAMs and random forests. For the GAMs, poverty status	
has the most significant impact, while traffic proximity and volume have the most significant	
impact for the random forests for the full indicator set. Regarding the PCs, the first PC has	
the most significant effect on model performance for both the GAMs and random forests.	30
3.9 West Representative Tree	
A representative tree from the West random forest model. The high energy burden nodes	
are in red, while the low energy burden nodes are in pink (in percentile). The root node, or	
starting point, is the largest to signify importance; each node, indicator split, decreases in	
size thereafter. Community resilience (the root node), median age, and air toxins related to	
respiratory risk greatly influence the high energy burden percentages.	31
3.10 Path to Knowledge Informed Policy	
An example of indicators and path-ways to design knowledge informed policy	34
4.1 Outage Duration Evaluation Criteria for the State of California	
4.2 Outage Duration Evaluation Criteria for Los Angeles County, CA	

4.3 Outage Duration Evaluation Criteria for Alpine County, CA . . . . .	40
4.4 Classification Model Evaluation Criteria for California Regions . . . . .	43
4.5 Methodology Overview . . . . .	47
4.6 LA Test Accuracy Across Varying Lead Times . . . . .	49
4.7 CO Test Accuracy Across Varying Lead Times . . . . .	50
4.8 Outage Forecasting Tool for Colorado. Each dot is a point in the 9km grid cell. A green dot indicates no risk, yellow dots are moderate risk, and red dots are high risk. The geographic bounding box for Colorado spans from 37.0°N to 41.0°N latitude and from 102.0°W to 109.0°W longitude. . . . .	53
5.1 Generation costs (left) and carbon emissions (right) per 15 minute period over a single day simulation for each of the three dispatch methods considered. . . . .	58

## **Chapter 1**

### **Introduction**

#### **1.1 Motivation**

#### **1.2 Research Questions**

This research seeks to answer the overarching question:

**How can we use machine learning and realistic grid modeling to design and operate power systems that are both climate-resilient and socially equitable?**

To address this, the dissertation proposal explores a series of targeted research questions, each corresponding to a chapter:

**Chapter 1:** What should modelers in the climate-energy nexus consider? How is climate change impacting power system infrastructure and operations?

**Chapter 2:** Who is disproportionately affected by high energy costs, and how can machine learning identify communities with elevated energy burden?

**Chapter 3:** Where and when will power outages occur during extreme weather events, and how long are these outages expected to last?

**Chapter 4:** Could we reduce carbon emissions through improved dispatch algorithms?

**Chapter 5:** How will an increase in solar power impact the Colorado power system under a changing climate?

These chapters are followed by **Chapter 6:**

### **1.3      Expected Outcomes**

## Chapter 2

### For the Reader: An Introduction to Weather Driven Power Systems

*This work is a shortened version of our paper: The climate-energy nexus: a critical review of power grid components, extreme weather, and adaptation measures, published in IOP Environmental Research: Infrastructure and Sustainability*

#### 2.1 Overview of Climate Modeling

This section provides insight into Global Climate Models (GCMs, also known as General Circulation Models) and emissions scenarios often used in climate-energy studies. With this knowledge, the reader can be further informed about scenarios used in previous works and scenarios that should be used in future works, considering climatic factors through a sensitivity, risk-based approach. GCMs are a starting point for the synergy between climate modeling and energy modeling, as energy modelers use GCM outputs, especially for future projections. Alternatively, historical data could be used. GCMs represent physical processes in the atmosphere, ocean, cryosphere, and land surface using physics-based equations and include information regarding atmospheric chemistry and aerosols, land surface interactions, and land and sea ice [34], [83].

A primary input for GCMs is the radiative forcing  $\frac{W}{m^2}$ , or forcing, the motivating factor behind climate change severity. Forcing is linked to the emission scenario selected, as the emission scenario provides a sequence of forcings. Forcings include changes in both shortwave radiation, i.e., the sun's output, and longwave radiation sources like Greenhouse Gases (GHG) such as  $CO_2$ , methane, nitrous oxides, halocarbons, and aerosols. Thus, they offer a physics-informed, risk-

based framework describing potential future outcomes relating to society and policy actions, their relationships to GHG, particulate matter, emissions, and their relationship to climate change. GCM use cases include the estimation of past forcings, using control runs that hold forcing constant to account for natural variability, and are substantially used for future climate sensitivity studies. Essential features of GCMs include spatial resolution and the time horizon (years) investigated in comparisons [70].

### 2.1.1 Emission Scenarios

Beginning in the year 2000, the IPCC used the Special Report on Emission Scenarios (SRESs) [84]. . .

In 2014, Representative Climate Pathways (RCPs) replaced SRESs. RCPs are classified based on the amount of forcing. They can conceptually be described as scenarios that relate concentration, emission, and land-use trajectories to provide information on possible development trajectories. AR5 was published in 2013 [41, 92].

In 2022, the IPCC Annual Report Six (AR6) was published, providing updated scenarios that should be used in studies moving forward. A key difference between the AR5 and AR6 is the data underlying climate projections and emissions for the AR5 Coupled Model Intercomparison Project (CMIP), version five, and for AR6, the CMIP6. CMIP6 uses updated RCP scenarios referred to as Shared Socioeconomic Pathways - Representative Climate Pathways (SSP-RCPs). SSP-RCPs can be thought of as RCPs, with additional data surrounding socioeconomic impacts relating to climate change and emissions [5]. Given the underlying differences in the RCPs and SRESs [78], this paper does not compare the scenarios. Still, rather an overview of emission projections for RCPs and SRESs is provided in Table 2.1.

Table 2.1: **Emission Scenario Categories From the IPCC**

This table presents Emission Scenarios from the IPCC fourth, fifth, and sixth reports. A.R. represents the IPCC Annual Report, paired with RCP for AR5 and AR6. Prior to RCPs, SRES were used in AR4.

Low Emissions	Medium Emissions	High Emissions
AR6 - RCP1.9	AR6 - RCP3.4	
AR6 - RCP2.6	AR6 - RCP4.5	AR6 - RCP8.5
AR5 - RCP2.6	AR5 - RCP4.5	AR5 - RCP8.5
SRES A1T	AR5 - RCP6.5	SRES A1F1
SRES B1	SRES B2	SRES A2
	SRES A1B	

The selection of emission scenarios should be made with caution. For instance, RCP8.5 was created to examine an unlikely high-risk future but was frequently used as a “business as usual.” scenario [35]. While there is merit to considering extreme scenarios, such as general preparedness for extreme events that may be better captured using a high-risk scenario, a con is that it may be harmful to near-term climate strategies, downplaying current adaption requirements for resilient infrastructure. Similarly, only studying the best-case scenario would consider the opposing extreme when the more likely scenarios are in-between [35, 70]. The International Energy Agency mapped the current policy scenario through an energy-related lens and found weak mitigation (SSP4-RCP6.0) as the most likely scenario [43].

### 2.1.2 Risk-Based Approaches

Risk-based approaches consider the relative likelihood of scenarios directly corresponding to direct risk, such as an increase in global temperature and systematic risk. Moving toward risk-based approaches would benefit those, including energy modelers, who are working on climate adaptation measures. A movement toward risk-based approaches would require climate experts to account for the relative likelihoods of the different outcomes [52]. It would require such experts to assign a probability to each scenario rather than having the scenario selected given climate outcomes, which is a multi-year effort. In the meantime, in-between scenarios should be more thoroughly explored [52, 35, 69].

The output of a GCM is an estimate of climate sensitivity, or how sensitive the earth is

to an increase in greenhouse gas concentrations, including climate feedback from the components discussed previously. GCM outputs include variables ranging from temperature and humidity for different layers of the atmosphere to the acidity (pH) and salinity at the ocean floor [35], [42]. A complete list of outputs may be found at [42].

### **2.1.3 Regional Climate Models**

More recently, Regional Climate Models (RCMs) have been investigated with energy-related works [100]. RCMs use downscaling of climate fields produced by GCMs. The need for downscaling stems from the need to get estimates of climate change at geographic scales, typically finer resolutions, that are relevant to energy simulations. Downscaling is achieved in two approaches: dynamic and statistical. Dynamic downscaling with RCMs is preferred given they honor the physics of the system. Still, they do introduce significant computational expense, whereas statistical downscaling is computationally cheap but has the tendency to basis correct, especially for highly localized regions which could infer statistical inference to the climate data [39].

Because of the physics parameterization, the uncertainty in downscaling is significant. Thus, tractable methodologies for sensitivity analysis are a substantial need in the climate modeling sector, giving further precedent to use dynamic methods [39], [99]. Although some research suggests the choice between statistical or dynamical approaches does not matter [64].

### **2.1.4 Power Sector Modeling**

When considering how climate data may be useful to an energy professional, it is important to understand the types of models generally used by energy practitioners. This section will focus on power sector modeling, given the focus of this research is the electrical power grid. However, other types of energy models exist, such as building energy models, which are reviewed in [15]. Additionally, [61] offers a review of current power sector modeling challenges and trends. For power sector modeling, there are four main types of models which include:

- (1) Data and Analysis Tools, studied in [63], [4], [9]

- (2) Capacity Expansion Models, reviewed in [91, 32, 9]
- (3) Production Cost (Grid Operations/Unit Commitment and Dispatch) Models, studied in [48, 30, 9]
- (4) Network Reliability Models, reviewed in [37, 80, 9]

For data analysis and tools, power system tracking and resource assessment could be completed. For instance, spatially and temporally explicit assessment of solar power under a future climate scenario could be explored. Capacity expansion models are a more advanced modeling tool that simulates transmission capacity and generation. Assumptions include “future electricity demand, fuel prices, technology cost and performance, and policy and regulation” [9]. Production Cost Models simulate a specific power system at a high temporal resolution but for a short period. Capacity Expansion outputs, such as generation and transmission capacity, emissions, or electricity prices, are inputs for production cost modeling. Network Reliability Models include Alternating Current (A.C.) power flow, which checks the steady-state operational feasibility of the network, as well as system dynamics and contingency events. For an in-depth review of model inputs and outputs, see [9]. Typically, model-related outputs would be used for extreme weather events, as observations are not always available and observed data may not be at a time-scale compatible with the power sector model. If observations were available, the observation data could be used as a calibration method for the climate model, whose output would be an input to the power sector model. For instance, a climate model could produce past and future data, and the past observed data could be used as a validation method. Alternatively, observed data could be used in a power sector model.

## 2.2 Extreme Weather Events

Climate change may impact the intensity and frequency of extreme weather, such as heat waves and cold fronts, and may exacerbate extreme events such as wildfires [21]. The National Oceanic and Atmospheric Administration (NOAA) reported that in 2023, the U.S. experienced 28

climate and weather-related events exceeding one billion or more losses in U.S. Dollars (USD). The 1990-2022 annual average was 7.9 events. Further, these events resulted in 492 deaths, the eighth highest amount of weather-related deaths in the CONUS since the 1980s [81, 72].

Power systems are vulnerable to drought [50, 86], water availability [94], flood [82], high wind [68, 57], high ambient air temperature [90, 17], wildfires [16, 85], and ice [27, 95]. Such vulnerabilities are troublesome to public use and financially burdensome, shown in Figure 2.1, and are likely to increase due to climate change.

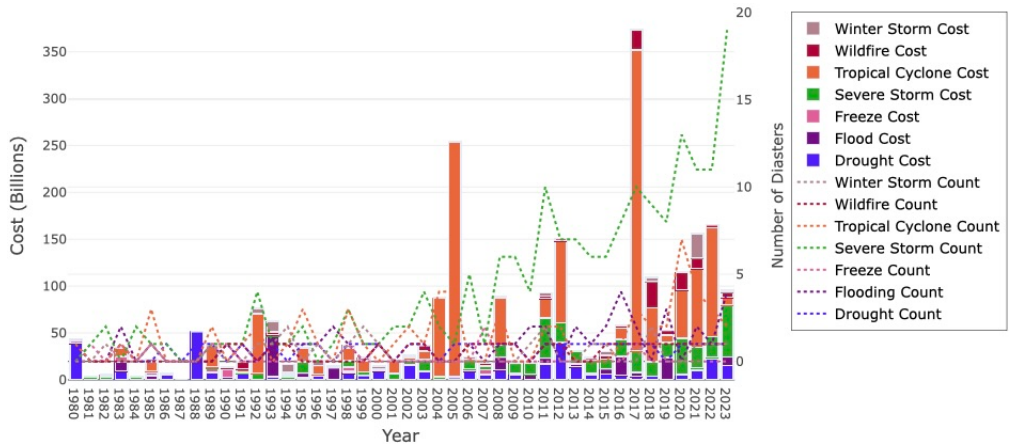


**Figure 2.1: U.S. Natural Disaster Occurrence and Cost since 1980**

The cost data is represented by the solid bars in USD and is Consumer Price Index adjusted. The event occurrences are presented by dashed lines for each year. Both cost and occurrence data are provided by [72]. A consistent increase in wildfire costs has been present since 2017. Tropical cyclone occurrence and cost do not correlate, while events such as drought and flood most commonly alternate over the years.

The urgency to understand extreme weather events and be proactive in upgrading aging power infrastructure is evident, considering that 83% of major reported power outages in the U.S. between 2000-2021 were attributed to weather-related events. Further, there was an increase of 64% more major reported outages in 2011-2021 than in 2000-2010, with approximately 78% of outages in 2011-2021 being caused by weather-related events, shown in Figure 2.2 [1].

### 2.2.1 Heatwaves

Heatwaves—defined as extended periods with daily maximum temperatures exceeding the norm by 5°C for five or more days [103, 66]—affect both power demand and infrastructure. Over-

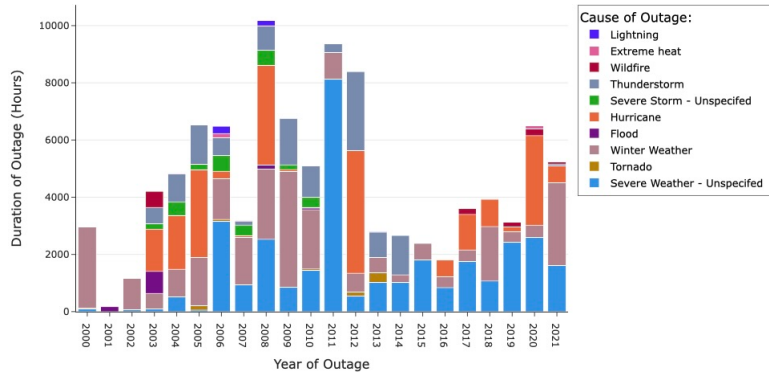


Figure 2.2: Duration of Major Power Outages in the CONUS

The power outage duration in hours shown per weather event for power outages impacting 500,000 customers or more between 2000–2021 [1].

head lines are rated based on historical temperatures, often limiting capacity under heat stress [51]. Transformers, sensitive to ambient conditions, may overheat when temperatures exceed their nameplate ratings [59]. Demand rises sharply due to air conditioning needs, with buildings accounting for over 75% of electricity use and cooling making up a major share [89]. Though direct heat-related outages made up only 1.9% of major outages from 2000–2021, their indirect strain is substantial.

### 2.2.2 Extreme Cold Temperatures

Despite warming trends, more intense winter events may occur due to Arctic disruption [77, 19, 18]. Cold conditions can cause ice build-up on lines, leading to faults from galloping conductors [73]. Substations face risks from increased soil resistivity and freezing conditions [36]. Winter storms raise demand and affect market prices through outages, generation losses, and fuel price spikes [60]. Snow, ice, and freezing rain contribute to 22% of weather-related outages.

### 2.2.3 Droughts

Droughts impact hydroelectric production by lowering reservoir levels, leading to dead pooling and operational limits [97]. Concurrent drought conditions across regions can strain multiple plants, increasing reliance on imports and blackout risk [94]. Additionally, 70% of U.S. generation relies on

cooling, with 48% needing freshwater [86], [24]. While droughts are rarely classified as direct outage causes, they indirectly influence grid stress, often paired with extreme heat [65].

#### **2.2.4 Non-Hurricane and Non-Tornadic Winds**

Extreme winds can damage infrastructure via conductor slap or by toppling vegetation onto equipment [55]. Wind also affects wind power generation, depending on direction and speed thresholds [58]. Climate models suggest stronger winds in the Central U.S. and reductions in coastal and western regions [23], [101]. Northeast utilities estimate that 38% of outages stem from wind, with restoration times averaging 8 hours.

#### **2.2.5 Wildfires**

The frequency and intensity of U.S. wildfires have grown, particularly in the West [28], [96]. Electric infrastructure is a major ignition source, particularly via vegetation contact or conductor slap [79], [45]. Wildfires accounted for 2.4% of major outages overall, with 65% occurring between 2017–2021. As events like the 2021 Marshall Fire show [8], longer fire seasons and increasing temperatures escalate grid vulnerabilities.

#### **2.2.6 Adaptation**

Table 2.2: **Common Power System Hardening Measures** [38, 76]

System hardening improves system infrastructure durability and stability, improving resilience and reliability through the lens of weather-related activity. System hardening is especially useful in existing power infrastructure. The measures provided are commonly implemented system hardening techniques.

Event	Hardening
Extreme Wind	Upgrading damaged poles and structures Strengthening poles with guy wires Burying power lines underground Vegetation management
Wildfires	Burying power lines underground Vegetation management Replacing wooden poles Installing wider cross-arms Replacing bare lines with insulated lines
Flooding	Elevating substations or control rooms Relocating or constructing new lines and facilities
Modernization	Deploying sensors and controls (smart grid technologies) Installing databases or tooling Replacing or upgrading aging infrastructure

**Table 2.3: Summarization of Adaptation Measures and Knowledge Gaps**

A summary of power system adaptation measures suggested for the future and knowledge gaps suggested for future studies.

<b>Extreme Weather Event</b>	<b>Adaptation Measure</b>	<b>Knowledge Gaps</b>
Heatwaves	<ul style="list-style-type: none"> <li>• Increase resource adequacy (including battery storage)</li> <li>• Demand response programs</li> <li>• Resource-sharing</li> <li>• Software upgrade related to operations</li> </ul>	<ul style="list-style-type: none"> <li>• Understanding the variability of both load and power transport regionally</li> <li>• Developing operational strategies that can minimize rolling blackouts</li> </ul>
Extreme Cold Temperatures	<ul style="list-style-type: none"> <li>• Weatherization</li> <li>• Resource adequacy</li> </ul>	<ul style="list-style-type: none"> <li>• Resource adequacy measures that consider the relationship between generator outages, generator maintenance, and temperature</li> <li>• Ice removal in unsafe conditions for crew dispatch and structural load changes</li> </ul>
Droughts	<ul style="list-style-type: none"> <li>• Retrofitting thermal gas plants to use water reuse strategies</li> <li>• Avoiding once-through cooling systems</li> <li>• Increasing monitoring of reservoirs and stream flows</li> <li>• Increasing power production efficiency</li> <li>• Increasing water storage capacity</li> <li>• Contingency plans</li> </ul>	<ul style="list-style-type: none"> <li>• Understanding regional interdependence on the power grid</li> <li>• Operational studies linking OPF programs with physics-based models, hydrologic/hydraulic models, RCMs, or system loadings with exogenous parameters across multiple time steps and regions</li> <li>• Resource adequacy</li> </ul>
Non-Hurricane and Non-Tornadic Extreme Winds	<ul style="list-style-type: none"> <li>• Frequent inspections</li> <li>• System hardening measures</li> <li>• Structural design considerations</li> <li>• Sensor technology to detect wind speeds at vulnerable power poles</li> <li>• Modernization</li> </ul>	<ul style="list-style-type: none"> <li>• Forecasting wind events</li> <li>• Methods for statistical analysis or downscaling methods for wind power generation installation and design, equipment cooling strategies, and infrastructure planning</li> <li>• Off-shore wind impacts for the CONUS</li> </ul>
Wildfires	<ul style="list-style-type: none"> <li>• Satellite imaging and sensing</li> <li>• Stationary and mobile ground-based technology</li> </ul>	<ul style="list-style-type: none"> <li>• Operational studies including metrics such as N-1 security</li> <li>• Optimizing PSPS on realis-</li> </ul>

When considering adaption measures, it is important to note that extreme events do not occur with equal frequency in areas of the CONUS or globally. Although, adaption measures for a weather-driven power system are crucial to the security of the power grid, critical infrastructure, and safety. A summary of the adaptation recommendations for the future, which includes system hardening techniques that are currently being implemented from Table 2.2, and knowledge gaps in the current literature are provided in Table ???. While each of the extreme events investigated in this review have unique characteristics, thus unique adaptation recommendations, it is evident that system hardening and weatherization are preliminary actions to consider in expanding and contributing to a robust grid in the face of climate change.

Modelers working at the climate-energy nexus must carefully consider the selection and application of climate scenarios, balancing probabilistic risk with scenario extremes, and integrating downscaled climate projections to capture regional impacts relevant to power systems. Climate change is already reshaping power infrastructure and operations through more frequent and severe extreme weather events—heatwaves, cold snaps, droughts, and high winds—that increase outage risks, strain equipment, and alter electricity demand patterns. Incorporating these dynamic climate impacts into power system models is essential for developing resilient, adaptive energy infrastructure and ensuring reliable electricity supply under uncertain future climates.

## Chapter 3

### For Frontline Communities: Energy Burden and Social Vulnerability in the Energy Transition

#### 3.1 Background

Energy and automation are foundational to the functioning and advancement of modern society. The U.S. comprises approximately 4% of the global population, yet it consumes around 101 quadrillion BTUs of primary energy annually, which accounts for nearly 17% of global energy consumption [3]. This substantial demand sustains a wide array of essential services, including housing, healthcare, education, transportation, and communication infrastructure [11].

The accelerating impacts of climate change are intensifying stress on infrastructure, disproportionately affecting low-income and historically marginalized communities. While policymakers at various levels have acknowledged these disparities, developing comprehensive and equitable policies that address the intersection of energy access, climate adaptation, and social justice continues to be a complex and urgent challenge [33, 46].

Within the broader field of energy justice, energy burden has emerged as a salient metric. Defined as the proportion of household income spent on energy expenses which include electricity, natural gas, and alternative fuels, energy burden provides a quantifiable lens for assessing energy affordability:

$$\text{Energy Burden (\%)} = \frac{\text{Annual Energy Costs (\$)}}{\text{Gross Household Income (\$)}} \quad (3.1)$$

According to the U.S. Department of Energy, households spending more than 6% of their

income on energy are considered to experience a high energy burden, while a burden above 10% is considered severe [29]. These thresholds derive from federal affordability standards, which suggest that utility costs should not exceed 20% of housing expenses and housing itself should not exceed 30% of gross income [25].

As both an absolute and primary measure of energy poverty [20], energy burden has been widely adopted in policy and academic contexts due to its direct reliance on consumer-level data and its clarity in guiding threshold-based interventions. High energy burdens are associated with a range of negative outcomes, including restricted energy use, thermal discomfort, and financial trade-offs that jeopardize food security, healthcare access, and housing stability. These interconnected challenges, often described as “bundled burdens” amplify the cumulative risks faced by vulnerable households [54].

### **3.2 Study Regions and Data Explanation**

The analyses in this chapter focus on the contiguous United States, segmented by census regions. These regions, Northeast, South, Midwest, and West, were delineated by the U.S. Census Bureau in 1942 to provide a standardized geographic structure for statistical evaluations and data summarization [12]. They also help account for broad patterns in physical and cultural geography relevant to national-scale studies.

The data used is organized at the county level and includes variables in several categories: meteorological and spatial data, building stock characteristics, environmental justice indicators, community resilience metrics, outage frequency, and household energy burden. Climate-related inputs, such as average July temperature (used to represent summer conditions), were sourced from NOAA’s National Centers for Environmental Information. The county level energy burden is shown in Figure 3.1. A summary of the variables and sources used in this study can be found in Table 3.2.

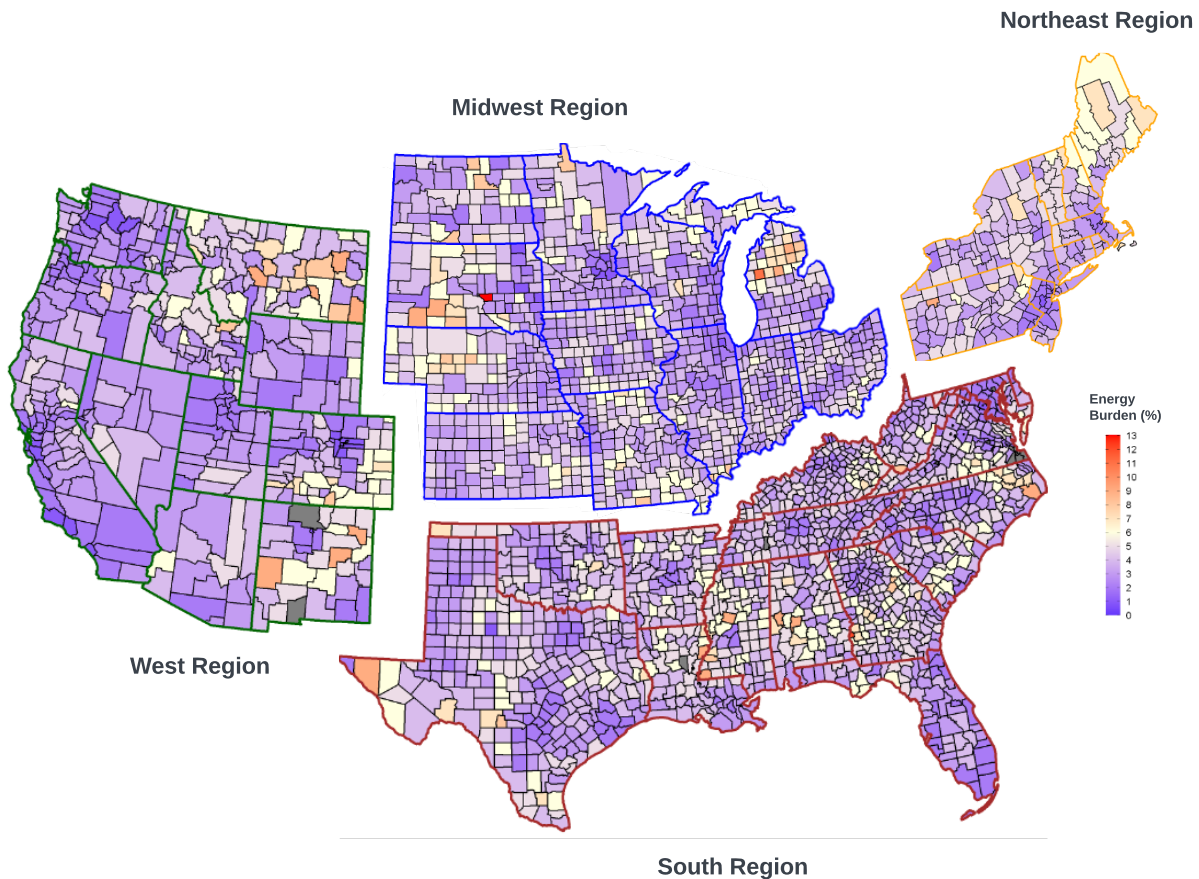


**Figure 3.1: County Level Energy Burden per Census Region**

The county level energy burden in each census region: west, midwest, south, and northeast. States outlined in green are the west region, states outlined in blue are the midwest region, states outlined in red are the south region, and states outlined in orange are the northeast region. An energy burden of 6% or higher is considered a high energy burden.

Table 3.1: Energy Burden Data Overview<sup>T</sup>

The data groups have been organized and labeled to support a clear discussion of the impact of energy burden indicators. The "Data Source" column identifies the original source and the corresponding group name, while the "Data Description" column provides a brief summary of the indicators included in each group.

Data Source	Data Description
Community Resilience for Equity and Disasters [87]	Estimated number of individuals with zero risk factors, Estimated number of individuals with one-two risk factors, Estimated number of individuals with three plus risk factors.
Socioeconomic Variables [88]	Total population count, Population for whom poverty status is determined, Count of households in linguistic isolation, Count of people of color individuals, Count of low-income individuals, Count of individuals age 25 or over with less than high school degree, Count of individuals under age 5, Count of individuals over age 64.
Environmental Justice Variables [88]	Count of housing units built before 1960, Diesel particulate matter level in air, Air toxics cancer risk, Air toxics respiratory hazard index, Traffic proximity and volume, Indicator for major direct dischargers to water, Proximity to national priorities list (NPL) sites, Proximity to risk management plan (RMP) facilities, Proximity to treatment storage and disposal (TSDF) facilities, Ozone level in air, PM2.5 level in air.
Location and Temperature [74]	Latitude and Longitude, Average daily temperature (July).
	A/C type in home

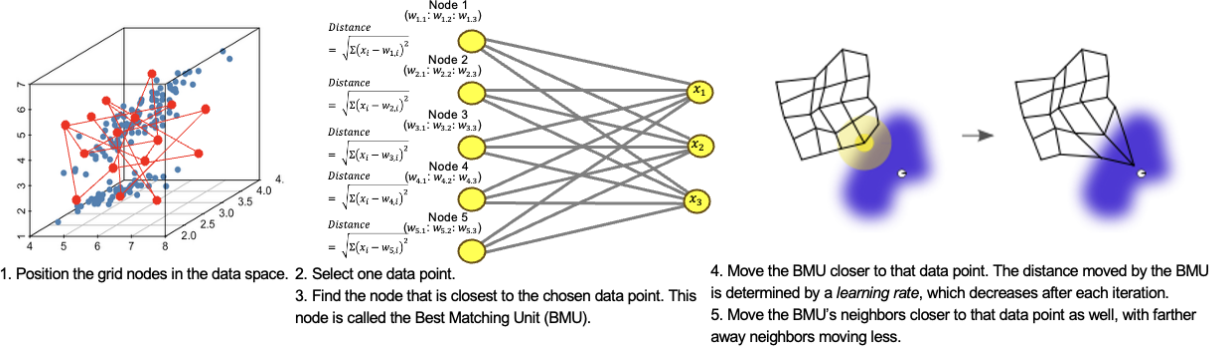


Figure 3.2: **The Self-Organizing Map Process** The five key step in the SOM process

### 3.3 Unsupervised Learning for Energy Policy Design: Insights from Self-Organizing Maps

The purpose of using unsupervised learning is to form groupings using general patterns and distributions related to indicators attributed to energy burden. *Prepared for journal publication.*

*Accepted to NeurIPS 2024 Workshop on Tackling Climate Change with Machine Learning.*

#### 3.3.1 Methods

A self-organizing map (SOM) is a form of unsupervised neural network based on competitive learning that has the capability to non-linearly map multi-dimensional data into two dimensions (2D). In Figure 3.2 the key steps of SOMs are explained. SOMs partition the data into nodes, which can be thought of as clusters, that are arranged in a 2D rectangular grid. This allows a SOM to embed a topological 2D manifold within a high-dimensional space (step 1). With each node, there is an associated weight vector; this corresponds to the node's position in the input space. Through an iterative process, for each data point,  $x_i$ , in the input data, the Euclidean distance to each node's weight vector is computed (steps 2 and 3). The node whose weight vector is most similar to  $x_i$  is called the Best Matching Unit (BMU). The weights of the BMU and nodes within its neighborhood radius are then adjusted toward the input data while the SOM nodes stay in a fixed position (steps 4 and 5). Given that the weight vectors in the input space move toward the input

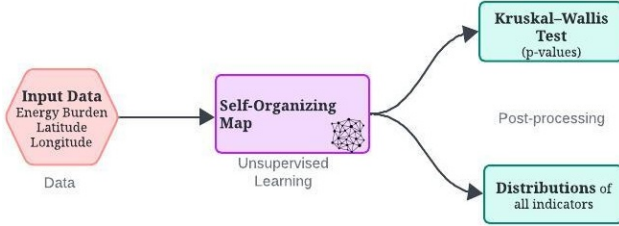


**Figure 3.3: Unsupervised Learning Methods**

The process begins with identifying the input data (red), then the SOMs are completed (pink), followed but the post-processing (blue).

data, a topological structure is naturally preserved and embedded. Other clustering algorithms, such as k-means, allow the data to move in clusters with no direct relationship to one another [? ]. The topological structure of SOMs is important, as counties near each other may have similar characteristics due to local and regional policy implications.

To date, SOM's have been implemented in energy related studies [? ? ] as well as studies investigating social-demographic disparities [? ]. For this study, energy burden, latitude, and longitude were the inputs to the SOMs, and the corresponding indicators were extracted using the latitude and longitude. Four SOMs were created, one for each census region. The number of nodes differs per census region, using a technique suggested by [93] in which the number of nodes is equal to the heuristic formula:  $5 \cdot \sqrt{n_{observations}}$ . The number of nodes, or grid size, was adjusted at times. The number of nodes was reduced because the SOM had missing nodes in these instances. The grid size selection is the most randomized step in the SOM process.

After the SOMs, each indicator and the partitioned SOM nodes are subjected to a Kruskal-Wallis test to determine whether that indicator has the same distribution across all SOM nodes. The Kruskal-Wallis test is a nonparametric equivalent to a one-way Analysis of Variance and is used in this study since it does not assume a normal distribution. To better understand indicator significance, p-values from the Kruskal-Wallis test are obtained and compared; in this study,  $p \leq 0.05$  is significant [? ]. Additionally, the distribution for each indicator is investigated per region and SOM node. This process is shown in Figure 3.3.1.

Table 3.2: Energy Burden Results Summary

A summary of the SOM results for each census region.

Census Region	SOM Topology	Low Energy Burden Nodes	Low Energy Burden Node Counties	Medium Energy Burden Nodes	Medium Energy Burden Node Counties	High Energy Burden Nodes	High Energy Burden Node Counties	Significant Indicators	High Energy Burden Counties	Count of Counties
West	3x4	7	298	4	71	2	43	41	54	412
Northeast	3x4	9	176	2	36	1	5	44	19	217
South	4x3	7	872	4	395	1	113	45	164	1380
Midwest	4x4	10	758	4	242	2	54	45	138	1054

### 3.3.2 Results

A full summary of SOM topology and indicator significance by region is presented in Figure 3.4 and Table 3.2. Across all four census regions, counties assigned to high energy burden SOM nodes consistently exhibited elevated values in air quality degradation, socioeconomic vulnerability, educational disparities, and housing-related risks.

Select distributions are found for the the West, in Figure 3.5, where high-burden nodes were associated with older populations, higher poverty rates, lower educational attainment, and significantly worse air quality—specifically diesel particulate matter, cancer and respiratory air toxics, and ozone levels. These areas also featured older housing stock, compounding vulnerability. While environmental justice indicators showed strong significance, variables tied to risk management facilities, water discharge, and hazardous waste proximity lacked consistent spatial patterns. Overall, 41 of 45 indicators showed statistically significant differences among SOM nodes.

## 3.4 Exploring the importance of Environmental Justice variables for predicting Energy Burden in the Contiguous United States

*This section has been published in iScience as a journal article titled: Exploring the importance of environmental justice variables for predicting energy burden in the contiguous United States.*

### 3.4.1 Methods

To enhance the understanding of influential indicators for predicting energy burden across the U.S., two modeling frameworks are developed and systematically compared. Both frameworks begin with an Exhaustive Subset Selection (ESS) procedure, employing a Branch-and-Bound algorithm

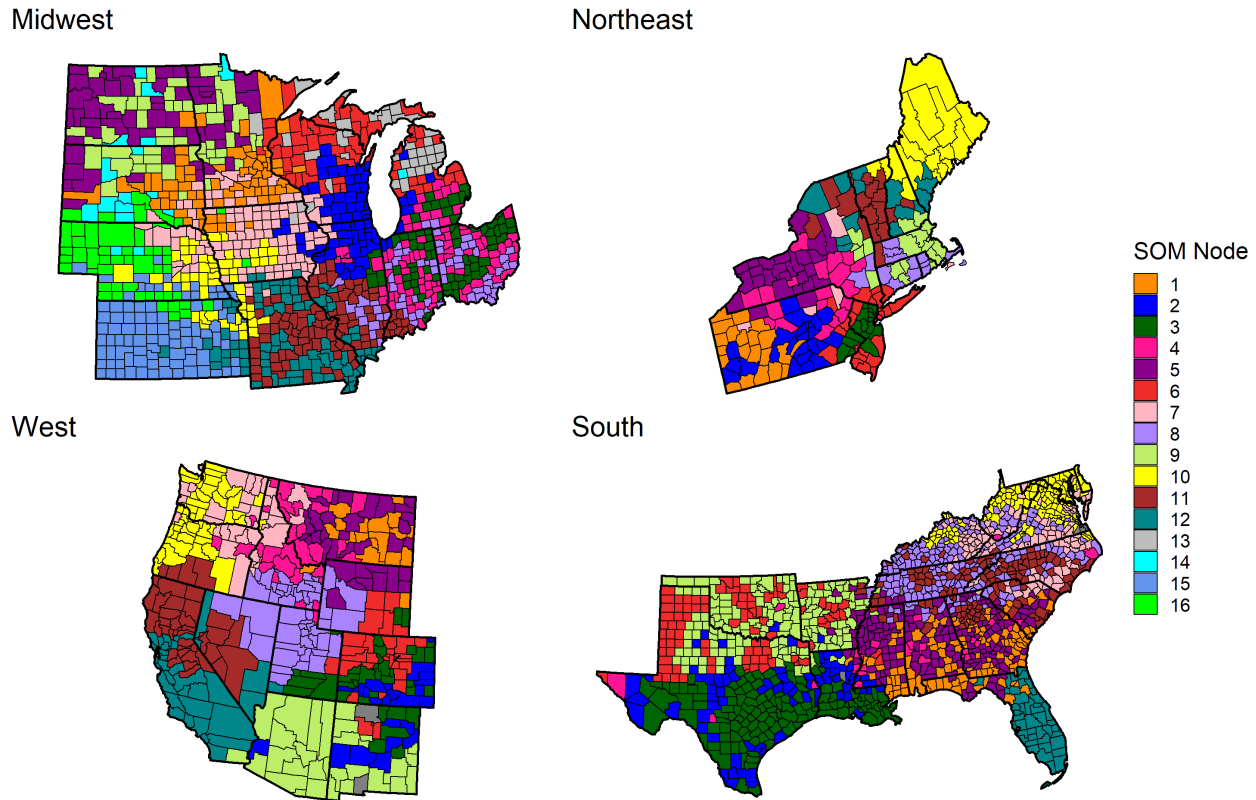


Figure 3.4: SOM Node Selection per Census Region

Each census region is shown at the county level, and the counties are categorized by the SOM node they were assigned to. The west and northeast both used a 3x4 topology, and the south used a 4x3, thus each of these regions have 12 nodes. The midwest used a 4x4 SOM topology and has 16 nodes.

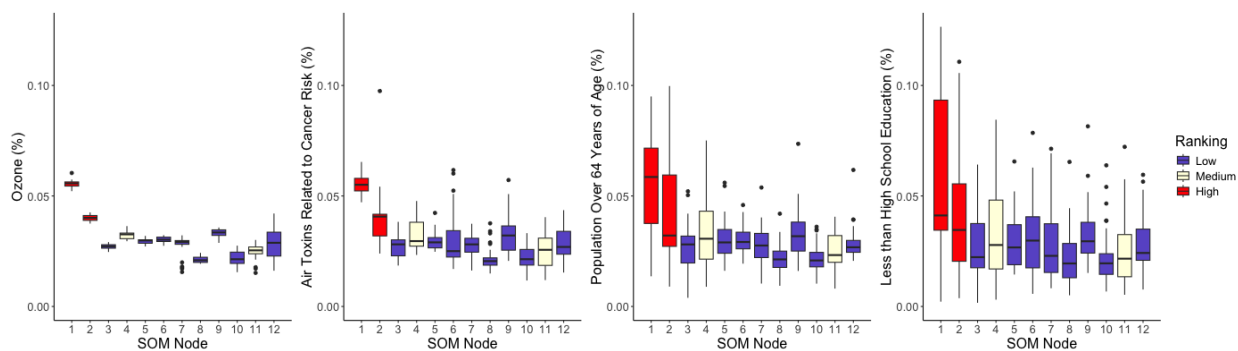


Figure 3.5: Distribution of Select Energy Burden Indicators

to identify the top 15 predictors from a broader set of variables based on their predictive strength for energy burden.

From the selected 15 predictors, all possible five-variable combinations are generated, resulting in 3,003 unique datasets. These serve as the basis for the subsequent modeling steps.

In the first framework, Generalized Additive Models (GAMs) are constructed using each of the 3,003 five-variable subsets, with 20 GAMs trained per subset, yielding a total of 60,060 models. From this set, the top 100 models are selected based on the lowest Generalized Cross-Validation (GCV) score. In the second framework, a random forest model is trained for each of the 3,003 datasets. The top 100 models are selected based on their coefficient of determination ( $R^2$ ). To enhance interpretability, a representative decision tree is extracted from the highest-performing random forest model.

For both modeling frameworks, a Leave-One-Column-Out (LOCO) analysis is applied to each of the top 100 models to assess the marginal contribution of individual predictors. Model performance is evaluated using multiple goodness-of-fit metrics, including the  $R^2$ , Root Mean Square Error (RMSE), and Mean Absolute Error (MAE).

Two types of datasets are used for comparison in both frameworks: (1) the full indicator dataset, comprised of all standardized county-level variables, and (2) a dimensionally reduced dataset created via Principal Component Analysis (PCA). The principal components represent linear combinations of the original variables that capture the majority of variance, supporting comparative model analysis with reduced complexity.

### 3.4.2 Results

The results presented are divided into two groups corresponding to the datasets used: the full indicator set or the PCs. Indicator groups are discussed to foster a more direct discussion around the indicators of energy burden used in this study. Indicator groups are provided in Table 3.2.

In order to gain a better understanding of indicator importance for knowledge-informed policy, first step was to perform a ESS to decrease the indictor set per region which is provided in

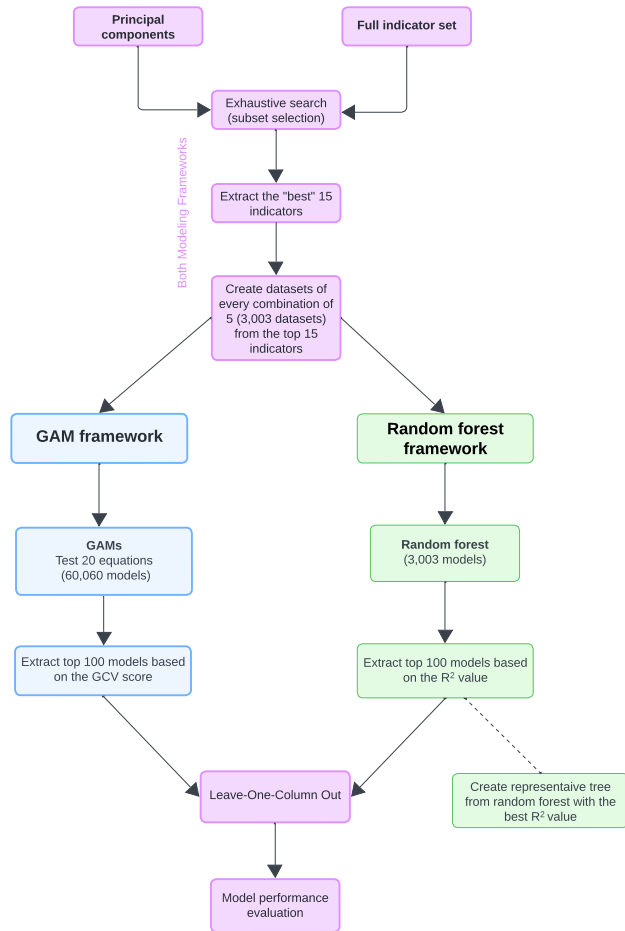


**Figure 3.6: Methodology Framework**

A brief description of the processes taken for each modeling framework. The pink represents processes applied to both modeling frameworks, while the blue is specific to framework one and the green is specific to framework two. Overall, two datasets, the full indicator set, and the principle components, are subjected to an exhaustive subset selection search. Then, 3,003 data sets are created from all combinations of 5 indicators. The data sets are then used in the GAM framework and random forest framework.

Table 3.3, then the indicators selected in the top 100 models for the GAMs and Random Forest are provided in Figure 3.7; the number of low-income individuals occurred in all of the top 100 models for each region. In comparison, the median age of individuals and poverty status occurred in the top 100 models for the West and Northeast. Additionally, population density occurred in each of the top 100 models for the Midwest. The West and Northeast share similar characteristics, while the South and Midwest have the most variability. For the random forest models, none of the indicators occurred in the top 100 models for every region. Thus, the random forest models are more distributed among the indicators than the GAMs. However, for both the random forests and GAMs, the Midwest shows similarities, as low-income individuals and population density are present in the top 100 models. One main takeaway is that with the ESS, the GAMs and random forests used the same 26 indicators out of the original 42 in the top 100 models. This is significant, as it provides a more tangible set of parameters to inform policy, reducing the parameter size by 16.

Although the PCA eliminates an aspect of model interoperability, both of the modeling frameworks use PCs to test the predictability of energy burden with less information loss. For the PCA, all 42 variables described in the “Data Description” from Table 3.2 are used. To better understand the indicator’s contribution to each PC, the absolute value of the magnitude of influence for each data group is provided in Table 3.4. The magnitude represents the influence indicators have within each PC. The first three PCs for each region were selected, given that this is when the variance explained by each subsequent PC began to drop off. For each region, the building characteristics had the most significant influence in the first PC, which is the most important PC as it will explain the greatest percentage of the data variance. Following the building characteristics are the socioeconomic variables and environmental justice variables. Among each region, within the first three PCs, the building characteristics, the socioeconomic variables, and the environmental justice variables are the primary influencers, meaning these data groups are represented more than their counterparts within the first three PCs.

The best model, according to the  $R^2$  value for modeling frameworks one and two are provided

**Table 3.3: Exhaustive Search Subset Selection Methods**

The indicators selected for each region from the exhaustive search subset selection using all data values.

Midwest	Northeast	South	West
Population	Poverty status	Low-income individuals	Poverty status
Low-income individuals	Low-income individuals	Traffic proximity and volume	Low-income individuals
Traffic proximity and volume	Median age	Poverty status	Median age
Median age	Air toxics respiratory hazard	Ozone level in air	Air toxics respiratory hazard
Proximity to risk management plan facilities	Natural gas consumption	Minority population	Natural gas consumption
1-2 Bedroom home	Propane consumption	Median age	Propane consumption
Households in linguistic isolation	Traffic proximity and volume	Households in linguistic isolation	Diesel particulate matter
Natural gas consumption	Diesel particulate matter	Population	Traffic proximity and volume
Fuel oil consumption	Ozone level in air	Mobile home	Community resilience: low risk
Power outage duration	Community resilience: low risk	Proximity to risk management plan facilities	Ozone level in air
Less than high school degree	Less than high school degree	Propane consumption	1-2 Bedroom home
Proximity to hazardous waste	1-2 Bedroom home	Air toxics respiratory hazard	Less than high school degree
Minority population	Multifamily housing	Less than high school degree	Multifamily housing
Air toxics respiratory hazard	Average power outage occurrence	Homes built prior to 1960	Households in linguistic isolation
PM 2.5 concentration	Households in linguistic isolation	Proximity to national priorities list sites	Homes built prior to 1960

**Table 3.4: Principle Component Analysis Magnitude**

For each region, the data groups are shown with their respective magnitude of influence within the first three PCs. The building characteristics, followed by the environmental justice variables, consistently show the most significant magnitude of influence within the first PC, which is the PC that explains the highest level of data variance.

Region	PC	Magnitude						Total Variance Explained
		Community Resilience	Socioeconomic Variables	Environmental Justice Variables	Location and Temperature	Building Characteristics	Power Outages	
Midwest	1	0.67	0.64	0.99	0.01	3.11	0.23	39%
	2	0.27	2.1	1.16	0.14	1.42	0.31	15%
	3	0.03	1.49	1.74	0.35	0.89	0.11	6%
Northeast	1	0.66	0.7	1.04	0.07	3.04	0.23	40%
	2	0.28	2.33	0.82	0.07	1.49	0.28	15%
	3	0.13	1.94	1.57	0.27	0.85	0.33	5%
South	1	0.69	0.55	0.82	0.03	3.11	0.25	38%
	2	0.14	2.52	0.79	0.06	1.15	0.19	12%
	3	0.03	1.18	1.84	0.19	0.82	0.08	7%
West	1	0.66	0.65	1.01	0.06	3.02	0.34	41%
	2	0.26	2.37	0.86	0.08	1.36	0.28	14%
	3	0.12	2	1.54	0.28	0.88	0.16	5%

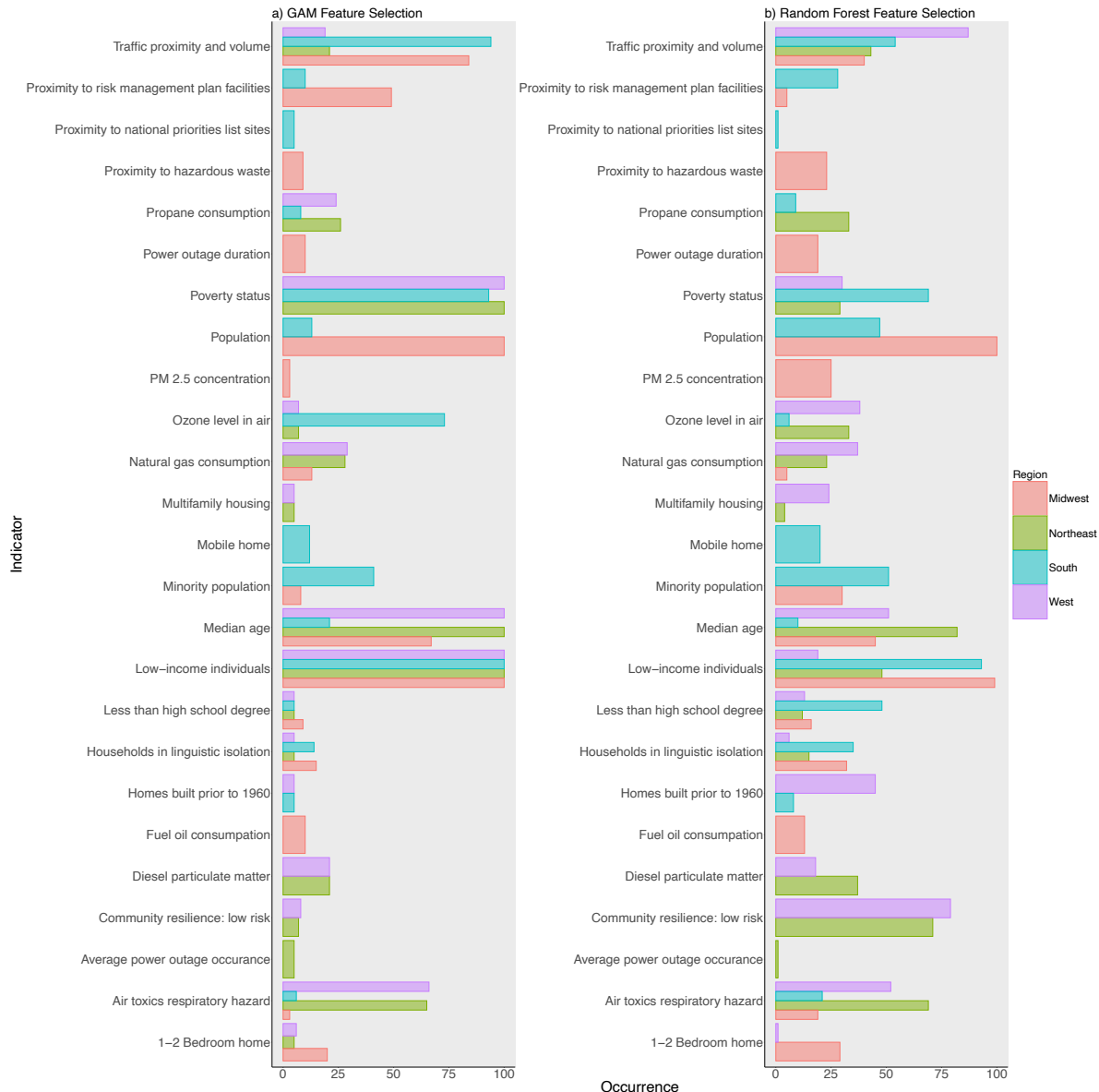


Figure 3.7: Modeling Method Variable Selection for the Top 100 Models

The variables that appeared in the top 100 models for each region using the full indicator set. Each region is assigned a color, while the bar width depends on the number of regions that include the variable. Each variable is given the same spatial width, but the individual bar size depends on the regions included.

for the energy burden full indicator set in Table 3.5 and the PCs in Table 3.6. Overall, the models using the PCs outperformed those using the full indicator set. This is to be expected as the PCA creates linear combinations of the original variables; thus, greater variance is captured using 5 PCs rather than using 5 indicators independently. For both the full indicator set and PCs, the GAM models outperformed the random forest models in terms of the  $R^2$  value, except for in the West region, using the full indicator set, which has the same  $R^2$  value of 0.84. For the full indicator set, the MAE, which does not take into account the direction of the error, and RMSE show mixed results. In the Midwest and the West, the MAE is lower for the GAM, but for the Northeast and South, the random forest outperforms the GAMs. However, the random forest models outperform the GAMs in terms of the RMSE scores for all regions except the Midwest, where the GAM outperforms the random forest. For the PCs, the GAM models consistently have better MAE and RMSE values.

Random forests and GAMs are both additive in nature and handle non-linear relationships within the data. However, there are key differences that could result in the differences between model performance and feature selection. In the GAMs, the linear components are replaced with a smooth non-linear function. The additive component occurs as each individual, smoothed non-linear indicator is added together to create an estimate. In the random forest model, predictions are combined or added from a sequence of models (decision trees) to create a prediction. Additionally, random forests use bagging, meaning each of the decision trees is trained on a subset of the data. As part of the bagging, indicators that contribute more heavily to the prediction are often selected over those that contribute to noise or are insignificant. GAMs do not use bagging; rather, they use spline methods, typically smoothing splines. In their simplest form, smoothing splines estimate the functional relationship between an indicator, such as low income and energy burden. The indicator is then transformed by the functional relationship; this transformed indicator is then used in the prediction.

To provide an example of the LOCO and representative trees, the following results will show the West Region, with other regions provided in Appendix A. For the LOCO analysis, the results for

Table 3.5: **Energy Burden Full Indicator Set Best Models**

The model with the highest  $R^2$  value for each region and modeling framework using the full indicator set. The region, modeling method, and the indicators used are shown, with the corresponding  $R^2$ , RMSE, and MAE values. In terms of  $R^2$  the GAMs outperform the random forests in all regions except for the West region, which has the same  $R^2$  value. Regarding the MAE and RMSE, the best performing models show mixed results among the GAMs and random forests. Given the different modeling methods, indicators used, and regions, this table should not be used as a direct comparison.

Region	Model	Representative Model Indicators	$R^2$	RMSE (%)	MAE (%)
Midwest	GAM	Total Population, Low-Income Individuals, Traffic Proximity, Proximity to Risk Management Plan Facilities, Median Age	0.77	0.87	0.63
	Random Forest	Total Population, Low-Income Individuals, Traffic Proximity, PM 2.5 Concentration, Median Age	0.73	0.93	0.68
Northeast	GAM	Poverty Status, Low-Income Individuals, Air Toxics Respiratory Hazard, Traffic Proximity, Median Age	0.84	0.86	0.62
	Random Forest	Low-Income Individuals, Air Toxics Respiratory Hazard, Ozone Level in Air, Community Resilience: Low Risk, Median Age	0.81	0.57	0.45
South	GAM	Poverty Status, Minority Population, Low-Income Individuals, Ozone Level in Air, Traffic Proximity	0.78	0.77	0.58
	Random Forest	Poverty Status, Minority Population, Low-Income Individuals, Linguistically Isolated, Traffic Proximity	0.72	0.67	0.51
West	GAM	Poverty Status, Low-Income Individuals, Air Toxics Respiratory Hazard, Traffic Proximity, Median Age	0.84	0.85	0.62
	Random Forest	Homes Built prior to 1960, Air Toxics Respiratory Hazard, Traffic Proximity, Community Resilience: Low Risk, Median Age	0.84	0.81	0.64

the West region, provided in Figure 3.8, show that the most significant difference in  $R^2$  values for the GAM models is attributed to poverty status ( $p < 0.01$ ). At the same time, the random forest models indicate that community resilience: low risk ( $p < 0.01$ ) results in the greatest decrease in  $R^2$  value. Similar to the other region's PC results, the West region shows that the first PC results in the most significant drop in  $R^2$  value. The first PC explains 41% of the data, and the building characteristics and environmental justice indicators have the greatest magnitude of influence. The consistent effect of the first PC and the building characteristics, together with environmental justice indicators having the most significant influence, suggests that improving building efficiency and addressing environmental justice issues could reduce energy burden in low-income areas.

Given that random forests are a black box method that utilizes decision trees, and decision trees are considered a highly interpretable method, representative trees from the best performing random forest are provided in Figure 3.9. The West shows a strong influence from the median age, low-income individuals, and community resilience indicators.

**Table 3.6: Energy Burden Principal Component Analysis Best Models**

The model with the highest  $R^2$  value for each region and modeling framework using the PCs. The region, modeling method, and the indicators used are shown, with the corresponding  $R^2$ , RMSE, and MAE values. For PCs, the GAMs outperformed the random forests for each of the modeling metrics.

Region	Model	Representative Model Indicators (PCs)	$R^2$	RMSE (%)	MAE (%)
Midwest	GAM	1, 4, 7, 15, 20	0.90	0.57	0.44
	Random Forest	1, 4, 7, 8, 20	0.87	0.67	0.50
Northeast	GAM	1, 4, 6, 20, 22	0.91	0.66	0.52
	Random Forest	1, 4, 6, 15, 20	0.88	0.81	0.61
South	GAM	1, 3, 4, 9, 22	0.89	0.57	0.44
	Random Forest	1, 3, 4, 9, 20	0.88	0.62	0.46
West	GAM	1, 4, 8, 13, 19	0.92	0.62	0.48
	Random Forest	1, 4, 6, 15, 19	0.89	0.80	0.61

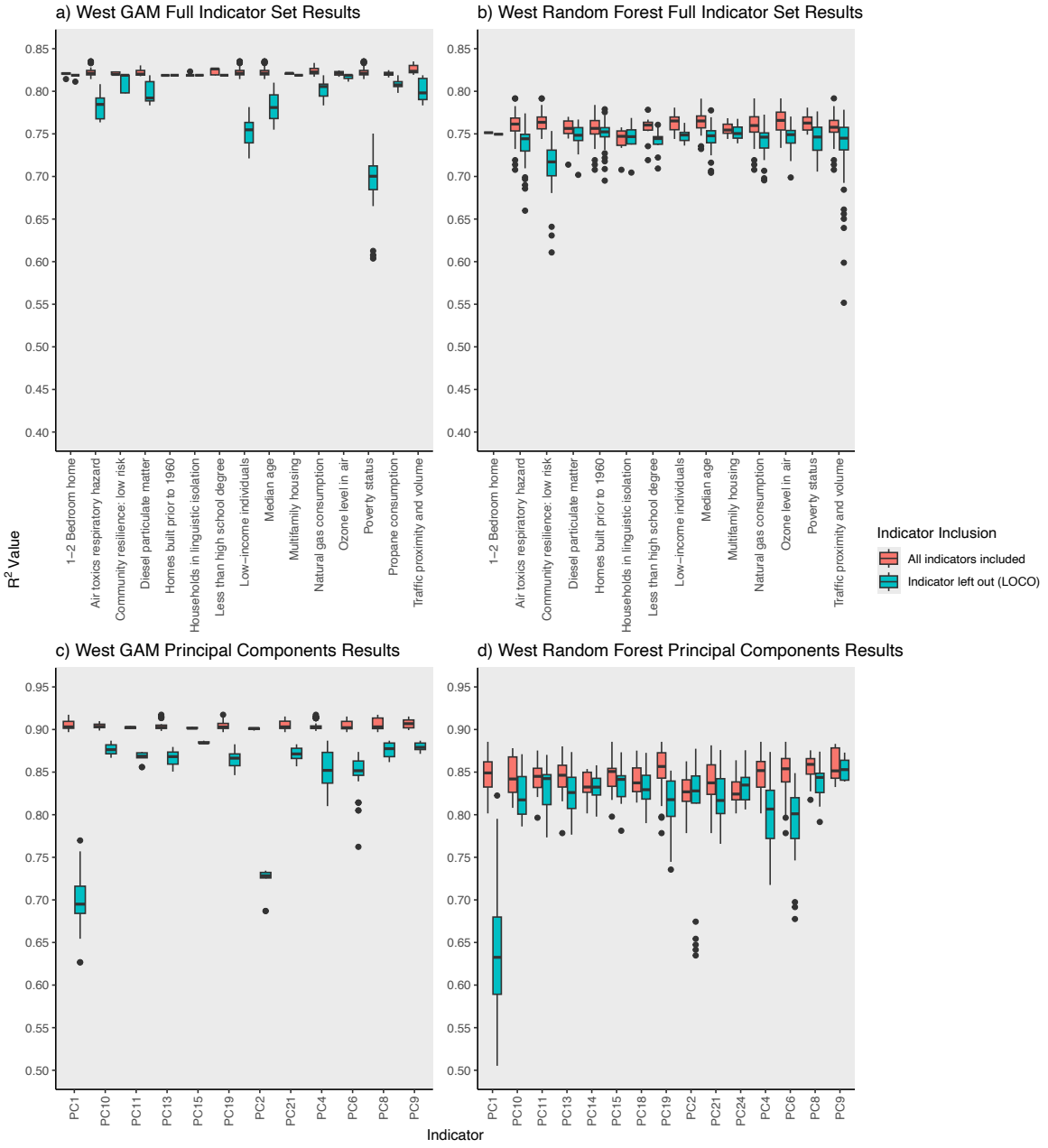


**Figure 3.8: Leave-One-Column-Out Analysis Indicator Influence for the West Region**

a) Represents the LOCO analysis for the GAM full indicator set in the South region b) Represents the LOCO analysis for the random forest full indicator set in the South region c) Represents the LOCO analysis for the GAM PCs in the South region d) Represents the LOCO analysis for the random forest PCs in the South region. Each indicator in the top 100 models for the GAMs and the random forest is subjected to a LOCO analysis. Here, the  $R^2$  value is provided for the entire model, meaning all the indicators for that model were included (red), and the LOCO model, meaning that one indicator was left out of the model (blue). The indicator dropped in the LOCO model is provided by the x-axis, and the change in  $R^2$  is presented on the y-axis. Poverty status, population, and low-income individuals have the most significant impact on the  $R^2$  value in both the GAMs and random forests for the full indicator set. Regarding the PCs, the first PC has the most significant effect on model performance for both the GAMs and random forests. For the GAMs, poverty status has the most significant impact, while traffic proximity and volume have the most significant impact for the random forests for the full indicator set. Regarding the PCs, the first PC has the most significant effect on model performance for both the GAMs and random forests.

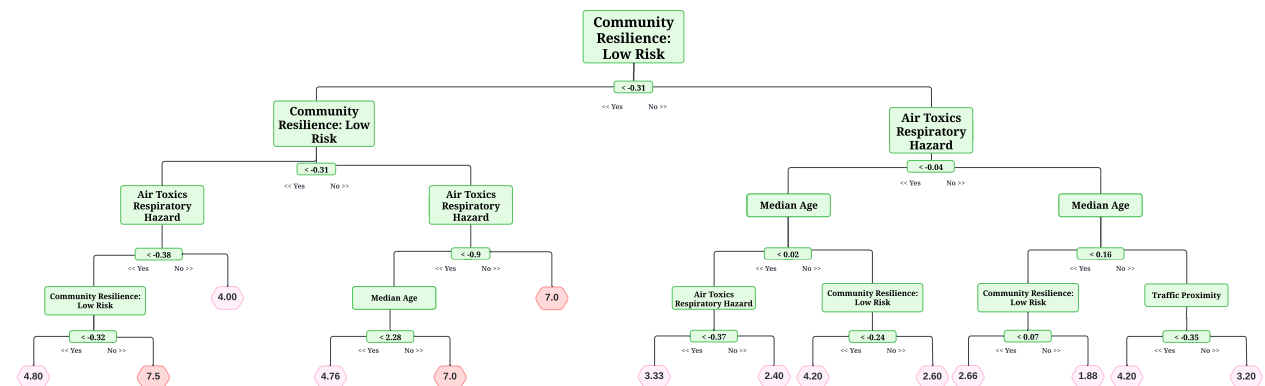


**Figure 3.9: West Representative Tree**

A representative tree from the West random forest model. The high energy burden nodes are in red, while the low energy burden nodes are in pink (in percentile). The root node, or starting point, is the largest to signify importance; each node, indicator split, decreases in size thereafter. Community resilience (the root node), median age, and air toxins related to respiratory risk greatly influence the high energy burden percentages.

### 3.5 Discussion

This chapter offers a dual-method exploration of energy burden in the United States, integrating both interpretable supervised machine learning models—Generalized Additive Models (GAMs) and Random Forests—and an unsupervised clustering approach using Self-Organizing Maps (SOMs). Together, these methods provide complementary insights into the complex, multi-dimensional nature of energy inequity across different U.S. census regions.

The supervised models were designed to identify the most influential predictors of energy burden at the county level. Across all regions, *poverty status* emerged as the strongest and most consistent indicator, affirming the relevance of financial assistance and energy efficiency programs. However, the results also highlighted the importance of less commonly addressed variables such as *air quality*, *housing age*, and *population density*, which point to structural and environmental vulnerabilities that require more systemic, long-term interventions.

Principal Component Analysis (PCA) reinforced that *building characteristics* and *environmental justice indicators*—particularly those related to air toxics and ozone levels—were among the most important contributors to model performance. LOCO (Leave-One-Column-Out) analysis further helped quantify the influence of individual features, offering a clear and interpretable basis for regional prioritization.

The SOM analysis extended these insights by revealing how energy burden clusters align with overlapping vulnerabilities across different geographies. High-burden SOM nodes consistently exhibited patterns of *elevated pollution exposure*, *aging housing stock*, *low educational attainment*, and disproportionate populations of elderly or young residents. In some cases, *linguistic isolation* and *minority status* emerged as additional drivers. These findings emphasize the importance of designing policy interventions that are both *spatially specific* and *culturally responsive*.

Finding suggest that communities disproportionately affected by high energy costs include those with older housing stock, poor air quality, higher poverty rates, low educational attainment, and aging populations—particularly in the West and Midwest. The different methods identified

high-burden communities were characterized by these vulnerabilities, enabling the spatial detection of counties where structural, socioeconomic, and environmental risks converge to elevate energy burden. Specific examples could include:

- In the Northeast, counties with high linguistic isolation may benefit from multilingual outreach programs.
- In the Midwest, areas with aging populations and outdated housing stock call for bundled retrofitting programs that integrate energy upgrades with health and safety improvements.
- In the South, communities heavily reliant on propane and natural gas—often low-income and minority populations—would benefit from fuel-switching incentives and solar-plus-storage programs.
- In the West, rural counties with poor air quality and low education levels underscore the need for air monitoring, energy literacy campaigns, and decentralized clean energy development.

Both studies also uncovered important outliers—counties with unique combinations of vulnerability that may be obscured in broader analyses. These include low-burden areas with industrial pollution or medium-burden clusters driven by isolated demographic stressors. However, the nexus between environmental justice, socioeconomic factors, housing, community resilience, and power outages are not always independently associated, and results from this study show they disproportionately impact counties that are already experiencing a high energy burden. Thus, results are advisable for creating knowledge-informed policy as shown in Figure ???. Such policies and the knowledge acquired through learning the indicators of energy burden create a path to climate action to avail and eliminate the compounded burdens of climate change on marginalized communities.

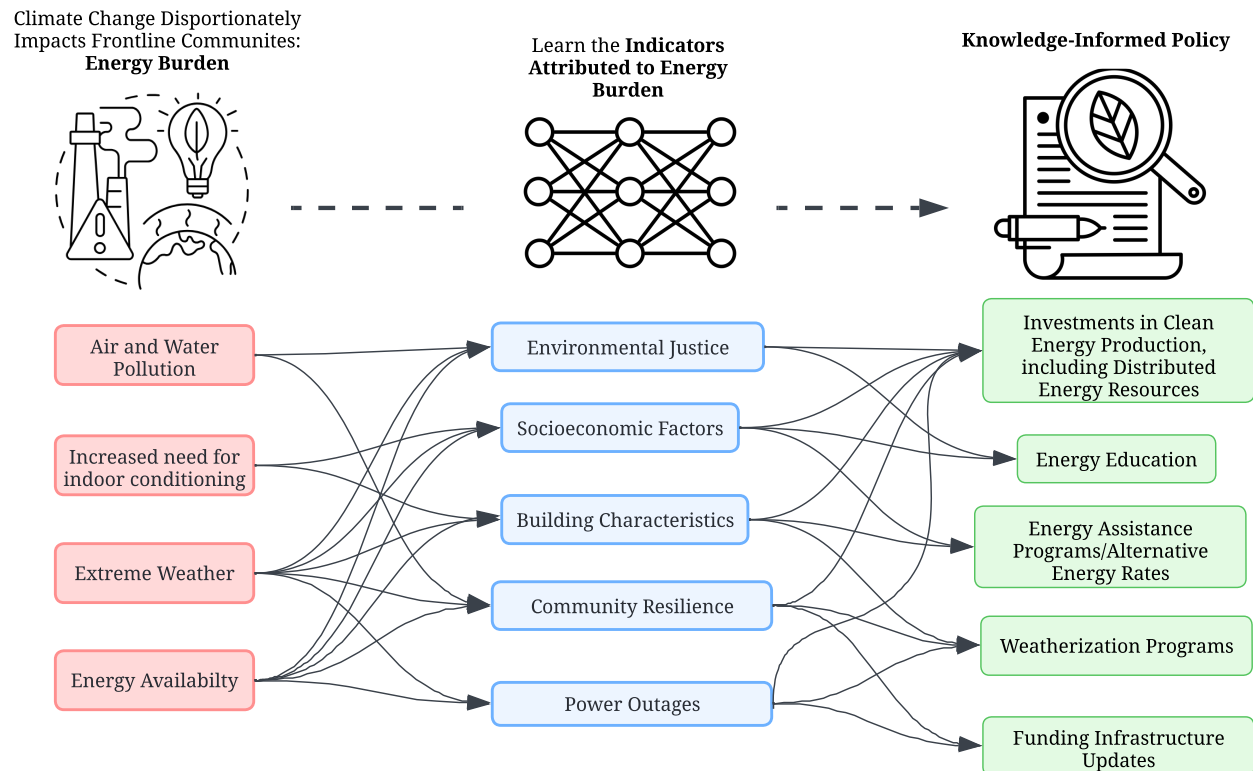


**Figure 3.10: Path to Knowledge Informed Policy**

An example of indicators and path-ways to design knowledge informed policy

## **Chapter 4**

### **For Proactive Grid Management: Forecasting Weather-Driven Power Outages and Duration**

#### **4.1 Introduction**

The rise of weather anomalies associated with climate change is projected to continue and intensify, posing escalating risks to critical infrastructure systems—including the electric power grid [21]. Extreme weather events, by nature, are difficult to predict. However, preparedness—through targeted forecasting and planning—can mitigate some of their most severe impacts, including physical damage to infrastructure, costly restoration processes, and disproportionate harm to vulnerable populations [22]. The financial implications are substantial: between 2019 and 2024, the United States experienced an average of \$151.2 billion in weather-related disaster costs annually.

Recent advancements in smart grid technologies and expanded access to high-resolution environmental and outage data have opened opportunities to apply machine learning (ML) and deep learning (DL) models to predict, manage, and reduce the consequences of power system disruptions. Despite this, a significant portion of the literature on grid resilience has focused on microgrid technologies, with relatively limited research applying ML to large-scale, weather-related outage prediction at finer spatial and temporal resolutions [47].

## 4.2 Learning to Predict Power Outage Durations from Historical Weather Data: Comparing Machine Learning Models

### 4.2.1 Study Region and Data

For numerical simulations, the power outage data was from [7], a service who scrapes publicly available utility outage data from power providers and aggregates the outages across the U.S. The timescale and granularity at which the outages were reported was utility-specific, but generally outage characteristics were reported on the minutes-level, which was then aggregated to hourly level data. For example, if an outage occurred for thirty minutes or longer within the hour, the occurrence equated to an outage (1), otherwise there was no outage for the hour (0). For the blackout duration data, the duration was calculated based on outage start and end times for every city-county pairing and then summed per county.

### 4.3 Methods

To support both restoration efforts and preparedness planning, this study applies a suite of machine learning models to predict power outage duration(regression) and power outage occurrence (classification) using historical weather data. Table 4.11 summarizes the modeling approaches and their corresponding prediction tasks.

Table 4.1: Regression and Classification Models Evaluated

Model	Dependent Variable
Multivariate Linear Regression	Outage Duration
Multivariate Logistic Regression	Outage Occurrence
Ridge Regression (Linear)	Outage Duration
Ridge Regression (Logistic)	Outage Occurrence
LASSO Regression (Linear)	Outage Duration
LASSO Regression (Logistic)	Outage Occurrence
Random Forest	Outage Duration
Stochastic Gradient Boosting (SGBoost)	Outage Duration
Adaptive Boosting (AdaBoost)	Outage Duration
Feedforward Neural Network (MFFNN)	Outage Duration
AdaBoost (Classification)	Outage Occurrence
SGBoost (Classification)	Outage Occurrence

All models, excluding standard linear and logistic regression, were tuned using five-fold cross-validation. The MFFNN employed hyperparameter optimization. Note that Random Forest and MFFNN were used exclusively for regression tasks in this study. Key hyperparameters tuned included:

- (1) LASSO and Ridge Regression: regularization strength ( $\lambda$ ).
- (2) Regression Trees: minimum samples to split a node, minimum samples per leaf, number of features considered, and maximum tree depth.
- (3) SGBoost: learning rate\*, number of estimators, number of features per split, and sample size\* for individual learners.
- (4) AdaBoost: learning rate\*, number of estimators, and loss function.
- (5) MFFNN: number of hidden layers and neurons optimized based on mean squared error.

(\* indicates parameters also cross-validated for classification tasks.)

An 80/20 train-test split was used for all models. For regression tasks, both time series and random splits were evaluated—reflecting differing assumptions about temporal dependence in outage duration. For classification tasks, only time series splits were used to maintain temporal integrity.

The regression models were assessed using: Root Mean Square Error (RMSE), Mean Absolute Error (MAE), and Mean Squared Error (MSE). The classification models were evaluated using: Accuracy, Precision, Recall and F1 Score. To further connect model results to grid reliability, we computed standard utility performance indices:

$$\text{SAIDI} = \frac{\sum \text{Outage Duration} \cdot \text{Number of Sustained Outages}}{\text{Number of Customers Served}} \quad (4.1)$$

$$\text{CAIFI} = \frac{\sum \text{Number of Outages}}{\text{Number of Customers Impacted}} \quad (4.2)$$

These metrics—System Average Interruption Duration Index (SAIDI) and Customer Average Interruption Frequency Index (CAIFI)—are widely reported by utilities and reflect performance over time [2]. Comparing predicted versus observed SAIDI and CAIFI provides insights into the real-world relevance of outage forecasting and the potential for proactive planning and investment in resilience.

#### 4.3.1 Results

#### 4.3.2 Power Outage Duration Prediction (Regression)

The power outage duration predictions among the cross-validated models for both CA and Los Angeles County, show a significantly better performance using the MFFNN as shown in Figures 4.1 and 4.2 for both the random data split and date-time split. For Alpine County, which had the smallest data set, the MFFNN had mixed results, shown in Figure 4.3. This provides insight that the MFFNN is better at generalizing among a larger region, or more populated region, where other models may need to be considered for small or rural regions.

For the state of CA, the MFFNN, trained using the date-time spilt, results in a testing RMSE of 0.792, MSE of 0.628, and MAE of 0.123, while the MFFNN using the random split results in a testing RMSE of 0.205, MSE of 0.0419, and MAE of 0.0578. While the Linear Regression, LASSO, and Ridge models performed almost identical among all metrics, with the Random Forest only performing marginally better considering the MAE. The Adaboost performed considerably worse among all metrics shown in Figure 4.1. The cross-validated model parameters for the date-time spilt are provided in Table ??.

The patterns for model performance in CA are also found for Los Angeles County. The MFFNN with the date-time spilt results in a testing RMSE of 0.122, MSE of 0.015, and MAE of 0.079, and the MFFNN using a random split results in a testing RMSE of 0.183, MSE of 0.0334, and MAE of 0.1451. The results show insignificant model performance differences among the other methods, with the Adaboost performing the worse, found in Figure 4.2. The cross-validated model

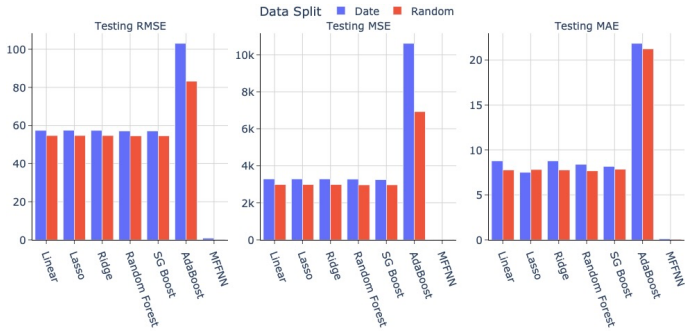


Figure 4.1: Outage Duration Evaluation Criteria for the State of California

parameters for the date-time date spilt are provided in Table ???. Regarding model performance, the weather variables and outage duration may not be have a linear relationship resulting in higher errors for the Linear, LASSO, and Ridge models. For the Adaboost and SG Boosting models, Adaboost implements a penalty term, whereas SG Boosting doesn't, making SG Boosting more flexible. However, if the data doesn't contain a high volume of noise or outliers, the penalty term may aid in better prediction capabilities.

For Alpine County the results were mixed, as the MFFNN outperformed the other methods using the random data split with a testing RMSE of 0.792, MSE of 0.628, and MAE of 0.123. While the MFFNN significantly outperforms the other models in all metrics except the MAE. However, when considering the date time data split, the MFFNN is the worst performing model, while the Adaboost model is the best performing among all models with a testing RMSE of 8.621, MSE of 74.327, and MAE of 0.4.890, resulting in the poorest performing “best” model for a selected location, provided in Figure 4.3. The cross-validated model parameters for the date-time date spilt are provided in Table ??.

Each model implemented cross-validation for the optimal hyper-parameters, however only the models using the date-time split are provided in this section as using past data to predict future power outage durations is more realistic in practice. Model hyper-parameters are provided in Tables ?? - ???. There are minor differences found between the state of CA and Los Angeles County. This could be explained by Los Angeles County making up approximately 19% of the CA

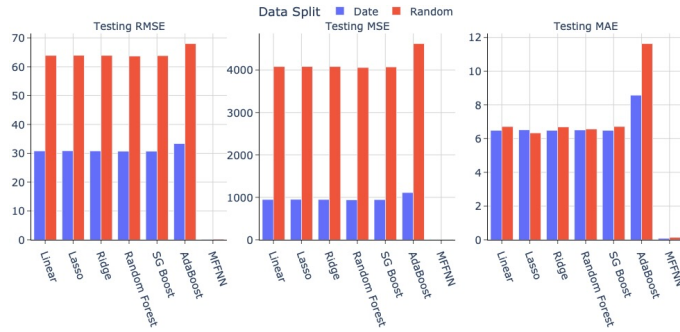


Figure 4.2: Outage Duration Evaluation Criteria for Los Angeles County, CA

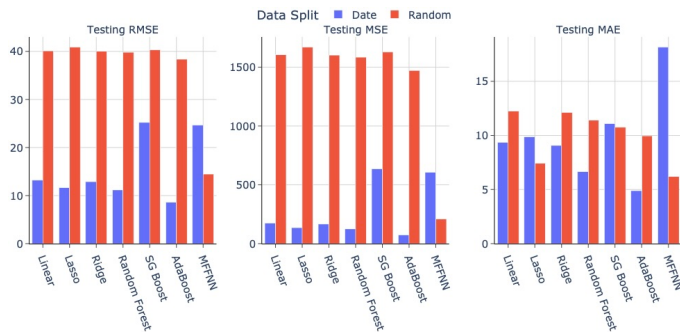


Figure 4.3: Outage Duration Evaluation Criteria for Alpine County, CA

data, while Alpine County only accounts for approximately 0.1%. The Ridge Regression model selected the same  $\lambda$  value for each region, while the Adaboost selected the same hyper-parameters for each region. However, the Adaboost model was the worse performing model for CA and Los Angeles County, but the best performing model for Alpine County.

Table 4.2: Hyperparameter Selection – California Date-Time Split

Parameter	Linear	Ridge	LASSO	RF	SGB	Adaboost	MFFNN
Lambda	-	8.701	0.751	-	-	-	-
Min Sample Split	-	-	-	45	-	-	-
Min Samples Leaf	-	-	-	6	-	-	-
Max Features	-	-	-	sqrt	log2	-	-
Max Depth	-	-	-	3	1	-	-
Learning Rate	-	-	-	-	0.15	0.06	0.001
Estimators	-	-	-	-	400	120	-
Subsample	-	-	-	-	0.8	-	-
Loss	-	-	-	-	-	square	-
Dense Layers	-	-	-	-	-	-	9

Table 4.3: Hyperparameter Selection – Los Angeles County Date-Time Split

Parameter	Linear	Ridge	LASSO	RF	SGB	Adaboost	MFFNN
Lambda	-	8.701	0.751	-	-	-	-
Min Sample Split	-	-	-	48	-	-	-
Min Samples Leaf	-	-	-	28	-	-	-
Max Features	-	-	-	sqrt	log2	-	-
Max Depth	-	-	-	9	1	-	-
Learning Rate	-	-	-	-	0.15	0.06	0.001
Estimators	-	-	-	-	400	120	-
Subsample	-	-	-	-	0.8	-	-
Loss	-	-	-	-	-	square	-
Dense Layers	-	-	-	-	-	-	8

Feature importance, particularly for the LASSO and Ridge models, is also a useful output to observe, since the  $L1$  and  $L2$  penalties serve as a method of feature selection. The wind speed, relative humidity, and temperature were found to have the most significant magnitude of influence when predicting power outage duration.

Table 4.4: Hyperparameter Selection – Alpine County Date-Time Split

Parameter	Linear	Ridge	LASSO	RF	SGB	Adaboost	MFFNN
Lambda	-	8.701	4.751	-	-	-	-
Min Sample Split	-	-	-	36	-	-	-
Min Samples Leaf	-	-	-	27	-	-	-
Max Features	-	-	-	sqrt	sqrt	-	-
Max Depth	-	-	-	2	7	-	-
Learning Rate	-	-	-	-	0.1	0.06	0.01
Estimators	-	-	-	-	700	120	-
Subsample	-	-	-	-	0.6	-	-
Loss	-	-	-	-	-	square	-
Dense Layers	-	-	-	-	-	-	5

### 4.3.3 Power Outage Occurrence Prediction (Classification)

For the power outage occurrence models the state of CA had a total of 3,682,587 hours of outages considering city-county pairing. Considering the date time split, the training set had 2,902,974 power outage occurrences (12% of the data), while the test set had 779,613 occurrences (13% of the data). For Los Angeles County, the training set had 506,259 power outage occurrences (16% of the data), while the test set had 133,665 occurrences (15% of the data), and for Alpine County the training set had 1,823 power outage occurrences (2% of the data), while the test set had 1,850 occurrences (9% of the data). The results for each model are provided in Figure 4.4.

For this set of models, predicting an outage occurrence was deemed of greater importance between the two classes. While the accuracy for the each model across each region individually shows minor differences, this may be misleading due to the imbalanced classes - there are significantly more hours without a power outages than with a power outage. Thus, to select the best model the recall and F1 Score were considered the most important.

For the state of CA, each model metric showed marginal differences among the methods applied, with the Logistic, LASSO, and Adaboost being almost identical in recall and F1 scores. Each model has a of recall of 0.006, F1 score of 0.012, 88% accuracy, but Logistic and LASSO model have a 0.262 precision, while the Adaboost model has a 0.300 precision. Thus, the Adaboost is determined to be the best model in this case. Los Angeles County finds the best model to be the

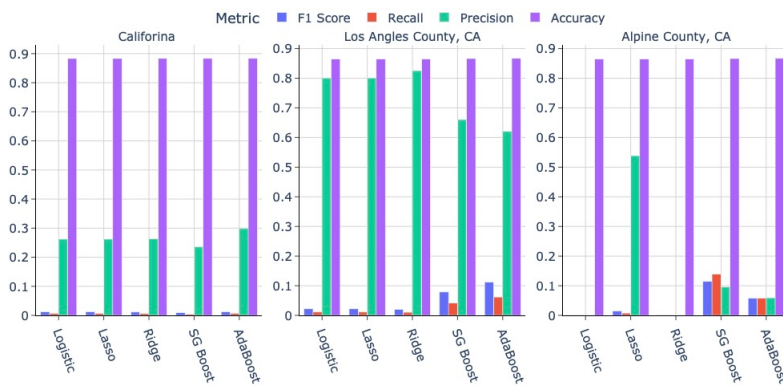


Figure 4.4: Classification Model Evaluation Criteria for California Regions

Table 4.5: State of California Outage Occurrence Hyper-Parameters

Model Hyper-Parameter	Ridge	LASSO	SG Boosting	Adaboost
Lambda	4.75	1.11	-	-
Max Depth	-	-	4	-
Learning Rate	-	-	0.05	0.01

Table 4.6: Los Angeles County Outage Occurrence Hyper-Parameters

Model Hyper-Parameter	Ridge	LASSO	SG Boosting	Adaboost
Lambda	4.75	1.11	-	-
Max Depth	-	-	4	-
Learning Rate	-	-	0.1	0.01

Adaboost, with a recall of 0.062, F1 score of 0.112, 87% accuracy and 0.62 precision. For Alpine County the best model is the SG boosting, with a recall of 0.140, F1 Score of 0.114, 86% accuracy and 0.100 precision. The cross-validated hyper-parameters for the classification models are found in Tables 4.5 - 4.7. Similar to the power outage duration, each region shows minor differences among the parameters selected.

Regarding feature importance, wind speed was found to be the most important feature for predicting a power outage occurrence across each region, when considering the LASSO and Ridge models. The power outage occurrence predictions proved to be more difficult to predict than

Table 4.7: Alpine County Power Outage Occurrence Hyper-Parameters

Model Hyper-Parameter	Ridge	LASSO	SG Boosting	Adaboost
Lambda	4.75	1.96	-	-
Max Depth	-	-	4	-
Learning Rate	-	-	0.05	0.01

Table 4.8: SAIDI Calculation for Test and Predicted Outage Durations

Model	Area	SAIDI Test	SAIDI Predicted
MFFNN	California	0.068	0.067
MFFNN	Los Angeles County	0.056	0.058
Adaboost	Alpine County	0.702	0.406

the power outage duration. This could possibly be due to the difference in model development for regression versus classification. But in addition, extreme weather can have a more direct relationship with outage time, given the need to bring in support crews from outside that immediate region. However, the best model for each region did use a boosting method, which are catered to imbalanced data sets, given their ability to resample the minority class. This provides insights to the types of models that can be considered in future studies.

#### 4.3.4 Reliability Metrics

To understand how predictive models can be useful to utilities, SAIDI is considered using the best models for each region predicting outage duration, shown in Table 4.8.

The SAIDI values using the MFFNN for CA and Los Angeles County result in essentially equal values, while the SAIDI value for Alpine County decreases, meaning the model predicted shorter durations than the true values. The SAIDI value for the test set is notably larger for Alpine County compared to CA and Los Angeles County, providing insight that the average duration of power outages are longer in Alpine County. The most logical ways to improve SAIDI is to either prevent an outage entirely or reduce the duration of the outage, likely through improved crew dispatch times. Thus, using predictive modeling could better prepare utilities and inform restoration efforts.

Table 4.9: CAIFI Calculation for Test and Predicted Outage Occurrence

Model	Area	CAIFI Test	CAIFI Predicted
Adaboost	California	0.022	0.004
Adaboost	Los Angeles County	0.056	0.156
SG Boosting	Alpine County	0.022	0.031

CAIFI is considered for power outage occurrence, shown in Table 4.9. Notably, Los Angeles County is the only region that the best model actually over-predicted the occurrence of an outage, resulting in a higher CAIFI value. Using weather variables to understand CAIFI could aid in preventing power outages that reoccur due to the same reasons, i.e. strong winds in a particular direction. This would allow for weather informed system hardening procedures.

## 4.4 Weather-Aware Predictions for Power Disruptions and Forecasting

### 4.4.1 Study Region and Data

For numerical simulations, the power outage data for LA County, CA was obtained from [7], a service that scrapes publicly available utility outage data from power providers and aggregates the outages across the U.S. The Colorado outage data was from INSERT CITE. The timescale and granularity at which the outages were reported was utility-specific, but generally outage characteristics were reported on the minutes-level. Meteorological variables were obtained from the Historical Weather API via Open-Meteo [102]. This dataset provides land variables at a spatial resolution of approximately 9 km, and an hourly temporal resolution, dating from 1940 to the present. The historical data was used for the model training and experimentation, and uses up to a 12-hour lead time, meaning that each weather variable up to 12 hours prior to time  $i$  is used to predict time  $i$ . To generate the negative samples, we performed random uniform spatiotemporal sampling dataset timeframe (2015-2021) to produce date-time and location pairs, there was an effort to maintain a balance of positive and negative samples given recent literature in imbalanced datasets [44, 53, 26], and as a first step in learning important weather indicators for predicting a power disruption. The

outage data was mapped to the weather data at hourly intervals. Open-Meteo additionally offers weather forecasting, which was used to implement the forecasting tool on the pre-trained models.

Table 4.10: Model Inputs: Meteorological Variables

Variable	Description
Temperature	Air temperature at 2m above ground (°C)
Precipitation	Total precipitation rate (rain + snowfall) (mm/h)
rain	Rainfall rate (mm/h)
snowfall	Snowfall rate (mm/h)
Surface pressure	Atmospheric pressure at surface level (hPa)
Wind speed	Wind speed at 10 m above ground (m/s)
Wind gusts	Max wind gust at 10 m above ground (m/s)
Wind direction	Wind direction at 10 m above ground (degrees)
Soil Moisture	Volumetric soil moisture 0–7 cm layer (m <sup>3</sup> /m <sup>3</sup> )
Cloud cover	Total cloud cover fraction (0–1)
Soil temperature	Soil temperature in top 0–7 cm layer (°C)
Terrestrial radiation	Downward longwave radiation at surface (W/m <sup>2</sup> )

#### 4.4.2 Methods

Power outage prediction is formulated as a classification task to support system operator preparedness. Various machine learning and deep learning models are trained using weather and environmental features, as summarized in Table 4.11. Random Forest and XGBoost models are optimized via five-fold cross-validation, while MLP and RNN use Hyperband, and the Transformer model is tuned with Optuna. A summary of key hyperparameters is provided below.

Following model training, we explore the influence of input features, particularly leading weather variables. Finally, the best-performing model is deployed in the outage forecasting tool **Ohmward**, as shown in Figure 4.5.

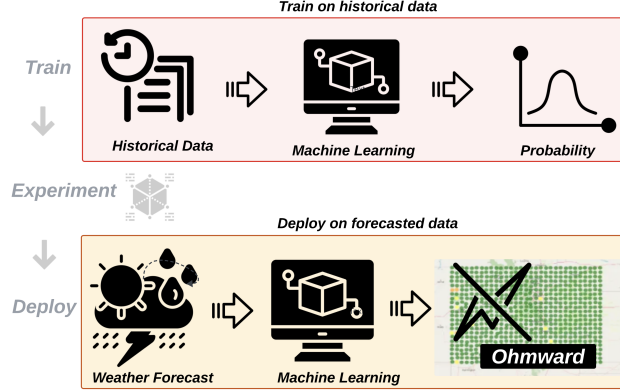


Figure 4.5: Methodology Overview

- (1) **MLP:** Hidden layers, activation functions, learning rate, units per layer, and dropout.
- (2) **Random Forest:** Number of trees, max features per split, min samples to split/leaf, and max tree depth.
- (3) **XGBoost:** Learning rate, boosting rounds, max tree depth, min child weight, subsample ratio, and feature selection per split.
- (4) **RNN:** Number of recurrent layers, hidden units, dropout rate, and batch size.
- (5) **Transformer:** Attention heads, encoder layers, dropout, learning rate, and batch size.

## Numerical Results

This section summarizes the predictive performance of the machine learning models for both Los Angeles County (LA) and the state of Colorado (CO). Across both regions, the Recurrent Neural Network (RNN) consistently achieved the highest test accuracy and balanced F1 scores, indicating strong capability in capturing temporal patterns relevant to power outages. In contrast, the Multilayer Perceptron (MLP) and Transformer models generally exhibited lower accuracy and higher variability, especially at longer lead times.

Figure 4.6 shows model performance in LA. Accuracy tends to plateau after a 6-hour lead time, suggesting that the most relevant weather patterns for outages are captured within that

Table 4.11: Hyperparameters Trained on 12-Hour Lead Times

Model	LA County, CA	State of CO
Random Forest	Split threshold: 22 Leaf size: 2 Max features: log2 Max depth: 9	
XGBoost	Subsample: 1.0 Estimators: 200 Min child weight: 1 Max depth: 7 Learning rate: 0.14	Subsample: 0.7 Estimators: 100 Min child weight: 1 Max depth: 4 Learning rate: 0.11
MLP	Layers: 4 Activations: ReLU and Sigmoid Learning rate: 0.0001 Units: 256 (all layers) Dropout: 0.1–0.5	Layers: 3 Activations: ReLU and Sigmoid Learning rate: 0.0008 Units: 128, 32, 32 Dropout: 0.1–0.5
RNN	Layers: 10 Activations: ReLU, Sigmoid, Tanh Dropout: 0.0–0.4	Layers: 10 Activations: ReLU, Sigmoid, Tanh Dropout: 0.1–0.2
Transformer	Attention heads: 8 Final MLP with ReLU and Sigmoid Layers: 1 Dropout: 0.28 Learning rate: 0.0008 Time & variable embeddings	Attention heads: 8 Final MLP with ReLU and Sigmoid Layers: 3 Dropout: 0.40 Learning rate: 0.89 Time & variable embeddings

window. In CO (Figure 4.7), performance trends are more mixed. The XGBoost and MLP models, in particular, show fluctuating accuracy, with some performance degradation at longer lead times. This may be due to a lower signal-to-noise ratio at those time horizons, as additional temporal inputs could introduce noise or spurious correlations.

Table 4.12 provides key evaluation metrics—test accuracy, F1 scores, and recall—for the best-performing configuration of each model. These results highlight each model’s strengths and limitations in capturing outage and non-outage events.

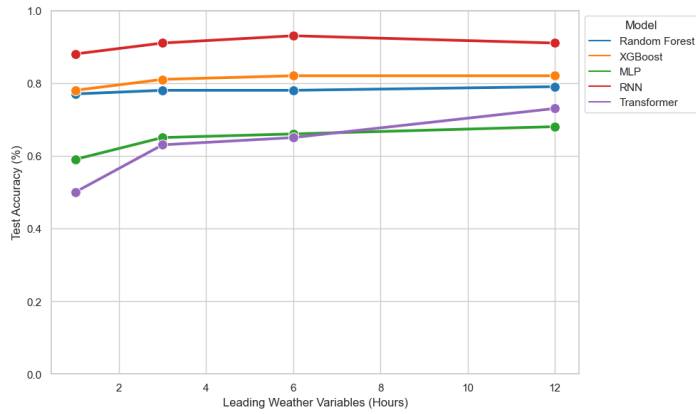


Figure 4.6: LA Test Accuracy Across Varying Lead Times

The RNNs’ strong performance underscores their ability to model temporal dependencies—essential for predicting weather-driven power outages. In both LA and CO, RNNs yielded high recall for outage events, which is especially important for operational forecasting. While Random Forest and XGBoost models showed slightly lower accuracy, they remained competitive and are appealing for their robustness and interpretability. XGBoost, in particular, performed reliably in both regions with minimal tuning.

By contrast, the MLP struggled with generalization. It showed poor recall for outages in LA and poor performance on non-outage events in CO. This could stem from its inability to model sequential dependencies in time-series data. Transformer models demonstrated moderate results; although they can handle temporal sequences using attention mechanisms, their performance was less stable and likely constrained by limited data and tuning. Given their complexity, further

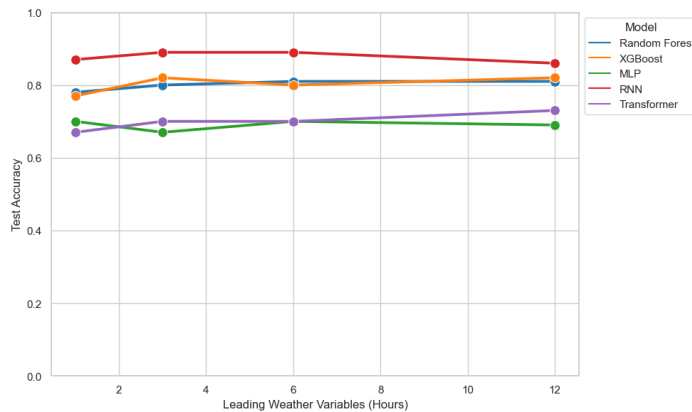


Figure 4.7: CO Test Accuracy Across Varying Lead Times

Table 4.12: Performance Metrics for Best Models by Region and Lead Time

Region	Lead Time	Model	Test Accuracy	F1 (0)	F1 (1)	Recall (0)	Recall (1)
LA	12	Random Forest	0.79	0.77	0.80	0.71	0.86
LA	12	XGBoost	0.82	0.81	0.83	0.79	0.85
LA	12	MLP	0.68	0.72	0.64	0.81	0.56
LA	1	RNN	0.92	0.90	0.90	0.89	0.93
LA	12	Transformer	0.64	0.73	0.46	0.98	0.31
CO	12	Random Forest	0.81	0.66	0.87	0.55	0.94
CO	12	XGBoost	0.82	0.69	0.87	0.61	0.92
CO	1	MLP	0.70	0.25	0.93	0.36	0.81
CO	6	RNN	0.89	0.79	0.91	0.70	0.97
CO	12	Transformer	0.73	0.37	0.83	0.24	0.97

optimization could improve their results substantially.

In summary, models that explicitly account for temporal structure—such as RNNs—generally outperformed those that treat observations independently. These results highlight the importance of model choice and lead-time configuration, especially when designing systems for predictive reliability in climate-sensitive power grids.

#### 4.4.3 Variable Importance

SHapley Additive exPlanations (SHAP) values were used to identify which weather features most strongly influenced outage predictions in LA County and Colorado. Across both regions, surface pressure and terrestrial radiation consistently ranked among the top five features, especially for lead times between 5–7 hours. These variables often pushed model predictions toward a higher likelihood of outage, suggesting a predictive window where meteorological signals are strongest.

High surface pressure, often linked to stable high-heat conditions, can increase electricity demand and strain infrastructure. Terrestrial radiation, which represents longwave energy emitted from the Earth’s surface, is higher during cloudless, hot days and may correlate with thermal stress on grid components.

Wind gusts also had a strong positive effect on outage probability, aligning with physical risks from sudden gusts impacting lines or vegetation. In contrast, low wind speeds tended to reduce outage risk, and wind direction did not show a clear pattern, potentially due to terrain effects in regions like Colorado.

At longer lead times (e.g., 12 hours), soil moisture and soil temperature emerged more frequently in top features. Their effects varied: low soil moisture may indicate drought and wildfire risk, while high soil moisture or frozen ground can cause vegetation stress or infrastructure failure during storms [44, 53, 26].

In sum, SHAP analysis offers both interpretability and operational insight by highlighting not just key variables, but also weather-driven mechanisms—heatwaves, storms, and wind events—that affect power system reliability.

#### 4.4.4 Implementation Example

Leveraging the insights from the model exploration, a public-facing web application powered by the XGBoost model, as a balance of accuracy and computational intensity, is deployed and shown in Fig 4.8. Because XGBoost demonstrated robust accuracy with up to twelve hours of historical data—and minimal gains beyond three hours, the service is configured to continuously ingest the forecasted 12 hours of meteorological observations and output the probability of an outage within the next 12 hours. The interactive map interface allows users to pan and zoom across Colorado, viewing real-time risk estimates at each grid point, by choosing XGBoost over the RNN, a lightweight yet accurate forecast engine that utilities and community planners can readily integrate into their decision-support workflow and use to gauge reliability metrics. The backend model could additionally be changed as research and computational resource availability increases. The application is publicly accessible at <https://ohmward.onrender.com> and is updated hourly as new weather data is forecasted.

#### 4.5 Conclusion

The integrated findings from these two studies offer a comprehensive perspective on the spatiotemporal occurrence and expected durations of power outages during extreme weather events, providing critical insights for improving grid resilience and informing mitigation strategies. In Los Angeles County, elevated surface pressure linked with heatwaves and associated increases in electrical load contribute to outages primarily concentrated in urban and peri-urban zones. Meanwhile, in Colorado, complex interactions between topography and weather variables create heterogeneous patterns of vulnerability, where dry soils and persistent radiation elevate wildfire risk and outage incidence.

Temporal modeling highlights that outage risk increases within a critical 12-hour window preceding extreme weather events, with predictive performance improving notably for lead times up to 6 hours. This temporal sensitivity aligns well with operational requirements for outage

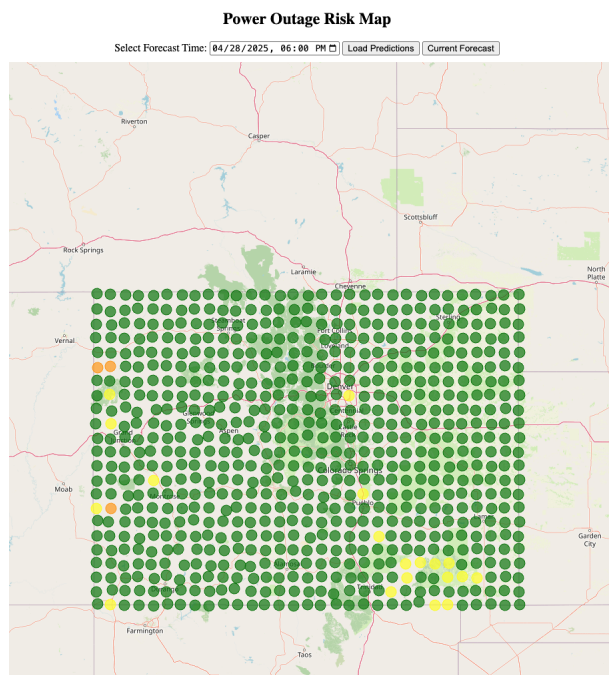


Figure 4.8: Outage Forecasting Tool for Colorado. Each dot is a point in the 9km grid cell. A green dot indicates no risk, yellow dots are moderate risk, and red dots are high risk. The geographic bounding box for Colorado spans from 37.0°N to 41.0°N latitude and from 102.0°W to 109.0°W longitude.

forecasting and emergency response planning. The first study uniquely advances understanding by explicitly modeling outage durations, an essential metric for assessing grid resilience and community impact. The use of deep learning architectures, MFFNN, demonstrates strong predictive capability for outage duration, revealing that outages range widely— from short disruptions lasting a few hours to prolonged outages extending multiple days.

Combining spatial-temporal outage duration predictions (Study One) with outage occurrence models (Study Two) enables a holistic understanding of where and when outages are likely to occur and how long affected customers might expect to be without power. This integrated approach facilitates enhanced situational awareness and supports prioritization of resources, enabling utilities to deploy crews strategically and allocate emergency services effectively.

Furthermore, the predictive frameworks developed in these studies, particularly the Ohmward system, offer practical avenues for operationalization. By coupling real-time meteorological forecasts with machine learning outage predictions, these tools provide actionable lead times (up to 6–12 hours) that can significantly reduce outage impacts through early intervention.

## Chapter 5

### For Power Grid Operations: Carbon-Aware Operational Strategy Evaluation

Many electricity system operators worldwide rely on approximate models to manage supply and demand efficiently. These models, especially the DC Optimal Power Flow (DC OPF), are embedded in large-scale optimization problems solved repeatedly throughout the day. DC OPF is a linear simplification of the more accurate but computationally intensive AC Optimal Power Flow (AC OPF), which fully captures the nonlinear, nonconvex behavior of electrical networks. While DC OPF offers fast computation and interpretability, it can yield physically unrealizable or economically suboptimal solutions [13], [6].

The canonical OPF problem aims to minimize the cost of active power generation while satisfying system constraints. However, due to the complexity of the AC OPF on large networks—often comprising tens of thousands of buses—many Independent System Operators (ISOs) implement DC OPF approximations, followed by an AC power flow (PF) step to validate feasibility. These approximations simplify voltage constraints, reactive power, and line losses, making them suitable for real-time operation [31]. Nevertheless, the resulting solutions can violate physical constraints, necessitating iterative re-solves [75], [49].

While the cost implications of such approximations have been studied, less is known about their impact on operational carbon emissions. This gap is significant as the power sector moves toward ambitious climate goals, such as a zero-carbon electricity grid in the United States by 2035 [67]. Typically, OPF formulations only consider generation cost and not the carbon intensity of different generator types. Because carbon emissions vary widely between technologies, generators

dispatched by cost-only OPF solutions do not necessarily minimize emissions [71].

The influence of OPF modeling decisions is growing in importance as grids integrate more variable renewable energy sources. Modern advances in solvers and computational resources now make high-fidelity OPF methods increasingly viable [40, 14]. While DC OPF remains attractive for its simplicity and speed, transitioning to AC OPF could reduce both cost and emissions—essentially enabling emissions mitigation through a “software upgrade.”

## 5.1 Test Cases and Grid Topologies

### 5.1.1 IEEE 118-Bus Test Case

### 5.1.2 United Kingdom

### 5.1.3 Electric Reliability Council of Texas

## 5.2 Dispatch Methods

### 5.2.0.1 AC Optimal Power Flow

The first method we consider is using AC optimal power flow (AC OPF), which is assumed to be the “ground-truth” model for how the power system behaves. This method generally considers a quadratic cost objective for generation, such that we aim to minimize:

$$f(P_g) = \sum_g c_{g_0} + c_{g_1} P_g + c_{g_2} P_g^2, \quad (5.1)$$

where  $c_{g_1}, c_{g_2}$  are the linear and quadratic cost terms of generator  $g$  respectively, and  $c_{g_0}$  are fixed costs. The constraints of the problem are the AC power flow constraints [14] which include constraints on bus voltage magnitude and thermal limits of lines and transformers. The thermal limits include both quadratic and multiplicative terms, thus resulting in a non-convex problem.

### 5.2.0.2 DC Optimal Power Flow

The second method we considered was DC optimal power flow (DC OPF) a commonly used first order approximation of the AC OPF problem which has been shown to provide a reasonable

representation of the power system under normal conditions [56]. Here we consider the same objective function (5.1) as above. One of the major assumptions of the DC OPF problem is the use of a linear approximation for the thermal limits while neglecting the voltage limits (as variables for voltage magnitude are not included). This means that the solution of the DC OPF necessarily does not satisfy the AC power flow constraints [6]. However, due to its convexity and significant computational benefits over AC OPF, this method is commonly used in practice. In order to solve the AC infeasibility of our DC OPF solution we run a power flow problem, where the generator outputs are fixed and a Newton-Raphson method is used to find a solution which satisfies the AC power flow constraints. In order to compensate for the difference in needed generation, a generator on the slack bus of the network (or slack buses) are used.

#### 5.2.0.3 DC Nearest Feasible Point

In this alternative method, we consider a dispatch which first uses DC OPF, but then finds the nearest AC feasible point. This method combines the dispatch decisions from the DC OPF problem, which are often used in ISO market clearings, with the physical feasibility of the AC OPF. Additionally, it allows us to comment on how the performance of the DC OPF dispatch is effected by the lack of feasibility. Here, we run a second optimization which seeks to minimize distance from the DC OPF dispatch, hence minimizing:

$$f(P_g) = \sum_{g=1}^{n_g} (P_g - P'_g)^2 \quad (5.2)$$

where  $P'_g$  are the DC OPF generator outputs. Expanding this equation and disregarding the constant terms (which have no impact on the optimal solution) yields:

$$f(P_g) = \sum_{g=1}^{n_g} P_g^2 - 2P'_g P_g. \quad (5.3)$$

This objective is minimized subject to the AC OPF constraints, which can be performed in PandaPower by adjusting the generator constant and quadratic objectives.



img/emisisons\_doubley.png

Figure 5.1: Generation costs (left) and carbon emissions (right) per 15 minute period over a single day simulation for each of the three dispatch methods considered.

### 5.3 Preliminary Results

Additionally, in Fig. 5.1, CO<sub>2</sub>e emissions per MWh are provided. This reiterates the findings from Fig. ??, and provides further context that, even when a larger generation capacity is needed, dispatch methods using a power flow correction result in a higher emissions per MWh of generation.

The cost per MW is also provided in Fig. 5.1, while the cost does not show significant differences per hour, the daily difference between AC OPF and DC OPF with AC PF results in a \$290,992.66 difference – and is expected to be higher for a higher demand day and larger network.

## **Chapter 6**

### **For Power System Planning in Colorado: Adapting Capacity Expansion to Climate Change and Solar Growth**

**6.1 Test Case**

**6.2 Methods**

**6.3 Simulation Evaluation**

## **Chapter 7**

### **Future Work**

- 7.1 For Power System Planning in Switzerland: Capacity Expansion under Climate Stress**
- 7.2 For Power System Modelers: Evaluating Topology and Dispatch Strategies with Realistic and Simplified Grid Models**
- 7.3 Research Plan**

## Bibliography

- [1] Surging Weather-related Power Outages | Climate Central.
- [2] IEEE Std 1366-2012, May 2012.
- [3] U.S. Energy Information Administration. What is the united states' share of world energy consumption? Available at <https://www.eia.gov/tools/faqs/faq.php?id=87&t=1> (2021/11/26).
- [4] Adil Ahmed and Muhammad Khalid. A review on the selected applications of forecasting models in renewable power systems. Renewable and Sustainable Energy Reviews, 100:9–21, February 2019.
- [5] Richard P Allan, Christophe Cassou, Deliang Chen, Annalisa Cherchi, L Connors, Francisco J Doblas-Reyes, Hervé Douville, Fatima Driouech, Tamsin L Edwards, Erich Fischer, Gregory M Flato, Piers Forster, Krishna M AchutaRao, Bhupesh Adhikary, Edvin Aldrian, and Kyle Armour. Summary for policymakers. page 32, 2023.
- [6] Kyri Baker. Solutions of DC OPF Are Never AC Feasible. In Proceedings of the Twelfth ACM International Conference on Future Energy Systems, e-Energy '21, page 264–268, New York, NY, USA, 2021. Association for Computing Machinery.
- [7] LLC Bluefire Studios. United states power outages. <https://poweroutage.us/>, 2022.
- [8] Boulder County Government. Marshall fire damage assessment list. <https://assets.bouldercounty.gov/wp-content/uploads/2022/01/marshall-fire-damage-assessment-list.pdf>, 2022.
- [9] Erin Boyd. Power sector modeling 101. Department of Energy – Office of Energy Policy and Systems Analysis, 2016.
- [10] Christa Brelsford, Sarah Tennille, Aaron Myers, Supriya Chinthavali, Varisara Tansakul, Matthew Denman, Mark Coletti, Joshua Grant, Sangkeun Lee, Karl Allen, Evelyn Johnson, Jonathan Huihui, Alec Hamaker, Scott Newby, Kyle Medlen, Dakotah Maguire, Chelsey Dunivan Stahl, Jessica Moehl, Daniel Redmon, Jibonananda Sanyal, and Budhendra Bhaduri. A dataset of recorded electricity outages by united states county 2014–2022. Scientific Data, 11(1):271, March 2024.
- [11] Marilyn A. Brown, Anmol Soni, Melissa V. Lapsa, Katie Southworth, and Matt Cox. High energy burden and low-income energy affordability: conclusions from a literature review. Progress in Energy, 2(4), 10 2020.

- [12] US Census Bureau. Geographic areas reference manual.
- [13] M. Cain, R. P. O'Neill, and A. Castillo. History of optimal power flow and formulations. FERC Technical Report. Last modified Aug. 2013.
- [14] Florin Capitanescu. Critical review of recent advances and further developments needed in ac optimal power flow. Electric Power Systems Research, 136:57–68, 2016.
- [15] Adrian Chong, Yaonan Gu, and Hongyuan Jia. Calibrating building energy simulation models: A review of the basics to guide future work. 253:111533, December 2021.
- [16] Moein Choobineh and Salman Mohagheghi. Power grid vulnerability assessment against wildfires using probabilistic progression estimation model. 2016 IEEE Power and Energy Society General Meeting (PESGM), page 1–5, July 2016.
- [17] Moein Choobineh, Paulo C. Tabares-Velasco, and Salman Mohagheghi. Optimal energy management of a distribution network during the course of a heat wave. Electric Power Systems Research, 130:230–240, Jan 2016.
- [18] J. Cohen, X. Zhang, J. Francis, T. Jung, R. Kwok, J. Overland, T. J. Ballinger, U. S. Bhatt, H. W. Chen, D. Coumou, S. Feldstein, H. Gu, D. Handorf, G. Henderson, M. Ionita, M. Kretschmer, F. Laliberte, S. Lee, H. W. Linderholm, W. Maslowski, Y. Peings, K. Pfeiffer, I. Rigor, T. Semmler, J. Stroeve, P. C. Taylor, S. Vavrus, T. Vihma, S. Wang, M. Wendisch, Y. Wu, and J. Yoon. Divergent consensuses on arctic amplification influence on midlatitude severe winter weather. Nature Climate Change, 10:20–29, Jan 2020.
- [19] Judah Cohen, Laurie Agel, Mathew Barlow, Chaim I. Garfinkel, and Ian White. Linking arctic variability and change with extreme winter weather in the united states. Science, 373(6559):1116–1121, Sep 2021.
- [20] Shuchen Cong, Destenie Nock, Yueming Lucy Qiu, and Bo Xing. Unveiling hidden energy poverty using the energy equity gap. Nature Communications, 13(1):2456, May 2022.
- [21] Dim Coumou and Stefan Rahmstorf. A decade of weather extremes. Nature Climate Change, 2(7):491–496, July 2012.
- [22] Rachel A. Davidson, Haibin Liu, and Tatiyana V. Apanasovich. Estimation of Post-Storm Restoration Times for Electric Power Distribution Systems, page 251–284. John Wiley Sons, Ltd, 2017.
- [23] K. Deng, W. Liu, C. Azorin-Molina, S. Yang, H. Li, G. Zhang, L. Minola, and D. Chen. Terrestrial stilling projected to continue in the northern hemisphere mid-latitudes. Earth's Future, 10(7):e2021EF002448, 2022.
- [24] Cheryl A. Dieter, Molly A. Maupin, Rodney R. Caldwell, Melissa A. Harris, Tamara I. Ivahnenko, John K. Lovelace, Nancy L. Barber, and Kristin S. Linsey. Estimated use of water in the United States in 2015, volume 1441 of Circular. Reston, VA, 2018.
- [25] Ariel Drehobl, Lauren Ross, and Roxana Ayala. How high are household energy burdens? American Council for an Energy-Efficient Economy, 2020.

- [26] Lindani Dube, Tanja Verster, Lindani Dube, and Tanja Verster. Enhancing classification performance in imbalanced datasets: A comparative analysis of machine learning models. *Data Science in Finance and Economics*, 3(4DSFE-03-04-021):354–379, 2023.
- [27] Melissa Dumas, Binita Kc, and Colin I. Cunliff. *Extreme Weather and Climate Vulnerabilities of the Electric Grid: A Summary of Environmental Sensitivity Quantification Methods*. Number ORNL/TM-2019/1252, 1558514. Aug 2019.
- [28] Matthew Dzaugis, Christopher W. Avery, Allison Crimmins, David R. Easterling, Kenneth E. Kunkel, Thomas K. Maycock, David R. Reidmiller, Brooke C. Stewart, and Russell S. Vose. Appendix 5: Frequently Asked Questions. Impacts, Risks, and Adaptation in the United States: The Fourth National Climate Assessment, Volume II. 2018.
- [29] Joel F. Eisenberg. Weatherization assistance program technical memorandum background data and statistics on low-income energy use and burdens. Available at <https://info.ornl.gov/sites/publications/Files/Pub49042.pdf>.
- [30] E Ela and M Milligan. Advanced unit commitment strategies for the u.s. eastern interconnection: Preprint. 2010.
- [31] Brent Eldridge, Richard O'Neill, and Anya Castillo. An improved method for the dcopf with losses. *IEEE Transactions on Power Systems*, 33(4):3779–3788, 2018.
- [32] L. Gacitua, P. Gallegos, R. Henriquez-Auba, Á. Lorca, M. Negrete-Pincetic, D. Olivares, A. Valenzuela, and G. Wenzel. A comprehensive review on expansion planning: Models and tools for energy policy analysis. *Renewable and Sustainable Energy Reviews*, 98:346–360, December 2018.
- [33] Oleg Golubchikov and Paola Deda. Governance, technology, and equity: An integrated policy framework for energy efficient housing. *Energy Policy*, 41:733–741, February 2012.
- [34] Great Lakes Integrated Sciences and Assessments. A practitioner’s guide to climate model scenarios, 2021.
- [35] Zeke Hausfather and Glen P. Peters. Emissions – the ‘business as usual’ story is misleading. *Nature*, 577(7792):618–620, Jan 2020.
- [36] Jinliang He, Rong Zeng, Yanqing Gao, Youping Tu, Weimin Sun, Jun Zou, and Zhicheng Guan. Seasonal influences on safety of substation grounding system. *IEEE Transactions on Power Delivery*, 18(3):788–795, Jul 2003.
- [37] Jun He, Zhijun Yuan, Xiaoling Yang, Wentao Huang, Yicong Tu, and Yi Li. Reliability modeling and evaluation of urban multi-energy systems: A review of the state of the art and future challenges. *IEEE Access*, 8:98887–98909, 2020.
- [38] Patricia Hoffman and William Bryan. Hardening and resiliency: U.s. energy industry response to recent hurricane seasons. <https://www.oe.netl.doe.gov/docs/HR-Report-final-081710.pdf>, 2010.
- [39] Mimi Hughes, Jessica D. Lundquist, and Brian Henn. Dynamical downscaling improves upon gridded precipitation products in the sierra nevada, california. *Climate Dynamics*, 55(1):111–129, Jul 2020.

- [40] M. Huneault and F.D. Galiana. A survey of the optimal power flow literature. *IEEE Transactions on Power Systems*, 6(2):762–770, May 1991.
- [41] Intergovernmental Panel on Climate Change. *Climate change 2014: synthesis report*. Geneva, Switzerland, 2015.
- [42] Intergovernmental Panel on Climate Change Working Group on Coupled Modelling. Cmip6 - coupled model intercomparison project phase 6f, 2019.
- [43] International Energy Agency. Data and projections - analysis and key findings. a report by the international energy agency, 2023.
- [44] Elaheh Jafarigol and Theodore Trafalis. A review of machine learning techniques in imbalanced data and future trends. (arXiv:2310.07917), October 2023. arXiv:2310.07917 [cs].
- [45] Saeed Jazebi, Francisco de León, and Albert Nelson. Review of Wildfire Management Techniques—Part I: Causes, Prevention, Detection, Suppression, and Data Analytics. *IEEE Transactions on Power Delivery*, 35(1):430–439, February 2020. Conference Name: IEEE Transactions on Power Delivery.
- [46] Sonal Jessel, Samantha Sawyer, and Diana Hernández. Energy, poverty, and health in climate change: A comprehensive review of an emerging literature. *Frontiers in Public Health*, 7, December 2019.
- [47] Fauzan Hanif Jufri, Victor Widiputra, and Jaesung Jung. State-of-the-art review on power grid resilience to extreme weather events: Definitions, frameworks, quantitative assessment methodologies, and enhancement strategies. *Applied Energy*, 239:1049–1065, Apr 2019.
- [48] Natalya Kalantayevskaya, Kairat Koshekov, Sergey Latypov, Alexey Savostin, and Kunelbayev Murat. Design of decision-making support system in power grid dispatch control based on the forecasting of energy consumption. *Cogent Engineering*, 9(1):2026554, December 2022.
- [49] Sung Min Kim, Kyri Baker, and Joseph Kasprzyk. Operational revenue insufficiency in highly renewable dc and ac-based lmp markets. In *2020 52nd North American Power Symposium (NAPS)*, pages 1–6, 2021.
- [50] T. A. Kimmell and J. A. Veil. *Impact of drought on U.S. steam electric power plant cooling water intakes and related water resource management issues*. Number DOE/NETL-2009/1364. April 2009.
- [51] Lamar Kimp, William Magee, Stephen Dasovich, Mark Shuck, Christian Sorensen, and Dmitriy Katsev. Guide for determination of bare overhead transmission conductors. page 47, 2019.
- [52] David King, Daniel Schrag, Zhou Dadi, Qi Ye, and Arunabha Ghosh. Climate change: A risk assessment - networks of evidence and expertise for public policy, 2015.
- [53] Corrado Lanera, Paola Berchialla, Abhinav Sharma, Clara Minto, Dario Gregori, and Ileana Baldi. Screening pubmed abstracts: is class imbalance always a challenge to machine learning? *Systematic Reviews*, 8(1):317, December 2019.

- [54] Jamal Lewis, Diana Hernández, and Arline T. Geronimus. Energy efficiency as energy justice: addressing racial inequities through investments in people and places. *Energy Efficiency* 2019 13:3, 13:419–432, 11 2019.
- [55] Gengfeng Li, Peng Zhang, Peter B. Luh, Wenyuan Li, Zhaohong Bie, Camilo Serna, and Zhibing Zhao. Risk analysis for distribution systems in the northeast u.s. under wind storms. *IEEE Transactions on Power Systems*, 29(2):889–898, Mar 2014.
- [56] Meiyi Li, Yuhan Du, Javad Mohammadi, Constance Crozier, Kyri Baker, and Soummya Kar. Numerical comparisons of linear power flow approximations: Optimality, feasibility, and computation time. In 2022 IEEE Power Energy Society General Meeting (PESGM), pages 1–5, 2022.
- [57] Si Han Li. Impact of climate change on wind energy across north america under climate change scenario rcp8.5. *Atmospheric Research*, 288:106722, June 2023.
- [58] Si Han Li and Gregory A. Kopp. Duration of extreme synoptic wind speeds for north america in a changing climate and its engineering implementation. *Structural Safety*, 104:102349, September 2023.
- [59] Xin Li, R.W. Mazur, D.R. Allen, and D.R. Swatek. Specifying transformer winter and summer peak-load limits. *IEEE Transactions on Power Delivery*, 20(1):185–190, 2005.
- [60] Jianing Lin, Minglei Bao, Ziyang Liang, Maosheng Sang, and Yi Ding. Spatio-temporal evaluation of electricity price risk considering multiple uncertainties under extreme cold weather. 328:120090, 2022.
- [61] Peter Lopion, Peter Markewitz, Martin Robinius, and Detlef Stolten. A review of current challenges and trends in energy systems modeling. *Renewable and Sustainable Energy Reviews*, 96:156–166, 2018.
- [62] Ookie Ma, Ricardo Oliveira Jon Weers Krystal Laymon, Megan Day, and Aaron Vimont. Low-income energy affordability data (lead) tool methodology. Available at <https://lead.openei.org/assets/docs/LEAD-Tool-Methodology.pdf> (2021/12/08).
- [63] R. Machlev, L. Heistrene, M. Perl, K. Y. Levy, J. Belikov, S. Mannor, and Y. Levron. Explainable artificial intelligence (xai) techniques for energy and power systems: Review, challenges and opportunities. 9:100169, August 2022.
- [64] R. Manzanas, J. M. Gutiérrez, J. Fernández, E. van Meijgaard, S. Calmanti, M. E. Magariño, A. S. Cofiño, and S. Herrera. Dynamical and statistical downscaling of seasonal temperature forecasts in europe: Added value for user applications. *Climate Services*, 9:44–56, Jan 2018.
- [65] Omid Mazdiyasni and Amir AghaKouchak. Substantial increase in concurrent droughts and heatwaves in the united states. *Proceedings of the National Academy of Sciences*, 112(37):11484–11489, Sep 2015.
- [66] Mark McCarthy, Lynne Armstrong, and Neil Armstrong. A new heatwave definition for the uk. *Weather*, 74(11):382–387, 2019.
- [67] McKinsey Insights: Electric power and natural gas. Net zero by 2035: A pathway to rapidly decarbonize the us power system, 10 2021.

- [68] Yousef Mohammadi Darestani, Abdollah Shafeezadeh, and Kyunghwa Cha. Effect of modelling complexities on extreme wind hazard performance of steel lattice transmission towers. *Structure and Infrastructure Engineering*, 16(6):898–915, Jun 2020.
- [69] M. Granger Morgan and David W. Keith. Improving the way we think about projecting future energy use and emissions of carbon dioxide. *Climatic Change*, 90(3):189–215, Oct 2008.
- [70] Richard H. Moss, Jae A. Edmonds, Kathy A. Hibbard, Martin R. Manning, Steven K. Rose, Detlef P. van Vuuren, Timothy R. Carter, Seita Emori, Mikiko Kainuma, Tom Kram, Gerald A. Meehl, John F. B. Mitchell, Nebojsa Nakicenovic, Keywan Riahi, Steven J. Smith, Ronald J. Stouffer, Allison M. Thomson, John P. Weyant, and Thomas J. Wilbanks. The next generation of scenarios for climate change research and assessment. *Nature*, 463(72827282):747–756, Feb 2010.
- [71] Martin Nicholson, Tom Biegler, and Barry W Brook. How carbon pricing changes the relative competitiveness of low-carbon baseload generating technologies. *Energy*, 36(1):305–313, 2011.
- [72] NOAA National Centers for Environmental Information. Noaa national centers for environmental information (ncei) u.s. billion-dollar weather and climate disasters (2023), 2023.
- [73] North American Electric Reliability Corporation. 2021 state of reliability an assessment of 2020 bulk power system performance. <https://www.nerc.com/pa/RAPA/PA/Performance>
- [74] Climate-National Oceanic and NOAA Atmospheric Administration.
- [75] Thomas J. Overbye, Xu Cheng, and Yan Sun. A comparison of the AC and DC power flow models for LMP calculations. In *37th Annual Hawaii International Conference on System Sciences*, Jan 2004.
- [76] Pacific Gas and Electric. Community wildfire safety program: Electric system hardening and vegetation management. [https://www.pge.com/pge\\_global/common/pdfs/safety/emergency-preparedness/natural-disaster/wildfires/fs-system-hardening.pdf](https://www.pge.com/pge_global/common/pdfs/safety/emergency-preparedness/natural-disaster/wildfires/fs-system-hardening.pdf), 2021.
- [77] Lennart Quante, Sven N. Willner, Robin Middelanis, and Anders Levermann. Regions of intensification of extreme snowfall under future warming. *Scientific Reports*, 11(11):16621, Aug 2021.
- [78] David R. Reidmiller, Christopher W. Avery, David R. Easterling, Kenneth E. Kunkel, Kristin L.M. Lewis, Thomas K. Maycock, and Brooke C. Stewart. *Impacts, Risks, and Adaptation in the United States: The Fourth National Climate Assessment, Volume II*. 2018.
- [79] B. Don Russell, Carl L. Benner, and Jeffrey A. Wischkaemper. Distribution feeder caused wildfires: Mechanisms and prevention. In *2012 65th Annual Conference for Protective Relay Engineers*, pages 43–51, April 2012.
- [80] Chanan Singh, Panida Jirutitijaroen, and Joydeep Mitra. *Electric Power Grid Reliability Evaluation: Models and Methods*. John Wiley Sons, December 2018.
- [81] Adam Smith. 2023: A historic year of u.s. billion-dollar weather and climate disasters, January 2024.

- [82] Laiz Souto, Joshua Yip, Wen-Ying Wu, Brent Austgen, Erhan Kutanoglu, John Hasenbein, Zong-Liang Yang, Carey W. King, and Surya Santoso. Power system resilience to floods: Modeling, impact assessment, and mid-term mitigation strategies. *International Journal of Electrical Power Energy Systems*, 135:107545, 2022.
- [83] Adam Terando, David Reidmiller, Steven Hostetler, Jeremy Littell, Douglas Beard, Sarah Weiskopf, Jayne Belnap, and Geoffrey Plumlee. Using information from global climate models to inform policymaking—the role of the U.S. geological survey. *2020–1058(2020–1058):32*, 2020.
- [84] The Intergovernmental Panel on Climate Change. *Emissions scenarios: summary for policymakers; a special report of IPCC Working Group III Intergovernmental Panel on Climate Change*. IPCC special report. Intergovernmental Panel on Climate Change, 2000.
- [85] Amarachi Umunnakwe, Masood Parvania, Hieu Nguyen, John D. Horel, and Katherine R. Davis. Data-driven spatio-temporal analysis of wildfire risk to power systems operation. *IET Generation, Transmission Distribution*, 16(13):2531–2546, 2022.
- [86] Union of Concerned Scientists. The ucs ew3 energy-water database — union of concerned scientists, 2012.
- [87] Community Resilience Estimates United States Census Bureau. About community resilience estimates. Available at <https://www.census.gov/programs-surveys/community-resilience-estimates/about.html> (2021/11/26).
- [88] EPA United States Environmental Protection Agency. Ejscreen: Environmental justice screening and mapping tool. Available at <https://www.epa.gov/ejscreen> (2021/11/26).
- [89] U.S. Energy Information Administration. Electricity explained: Use of electricity, 2022.
- [90] U.S. Government Accountability, Office. Climate change: Energy infrastructure risks and adaptation efforts — u.s. gao, 2014.
- [91] Jonas van Ouwerkerk, Hans Christian Gils, Hedda Gardian, Martin Kittel, Wolf-Peter Schill, Alexander Zerrahn, Alexander Murmann, Jann Launer, Laura Torralba-Díaz, and Christian Bubar. Impacts of power sector model features on optimal capacity expansion: A comparative study. *157:112004*, April 2022.
- [92] Detlef P. van Vuuren, Jae Edmonds, Mikiko Kainuma, Keywan Riahi, Allison Thomson, Kathy Hibbard, George C. Hurtt, Tom Kram, Volker Krey, Jean-Francois Lamarque, Toshihiko Masui, Malte Meinshausen, Nebojsa Nakicenovic, Steven J. Smith, and Steven K. Rose. The representative concentration pathways: an overview. *Climatic Change*, 109(1):5, Aug 2011.
- [93] J. Vesanto and E. Alhoniemi. Clustering of the self-organizing map. *IEEE Transactions on Neural Networks*, 11(3):586–600, 2000.
- [94] Nathalie Voisin, Ana Dyreson, Tao Fu, Matt O’Connell, Sean W. D. Turner, Tian Zhou, and Jordan Macknick. Impact of climate change on water availability and its propagation through the western u.s. power grid. *Applied Energy*, 276:115467, Oct 2020.

- [95] Fei Wang, Hanchen Xu, Ti Xu, Kangping Li, Miadreza Shafie-khah, and João P. S. Catalão. The values of market-based demand response on improving power system reliability under extreme circumstances. *Applied Energy*, 193:220–231, 2017.
- [96] A. Park Williams, John T. Abatzoglou, Alexander Gershunov, Janin Guzman-Morales, Daniel A. Bishop, Jennifer K. Balch, and Dennis P. Lettenmaier. Observed Impacts of Anthropogenic Climate Change on Wildfire in California. *Earth's Future*, 7(8):892–910, August 2019. Publisher: John Wiley & Sons, Ltd.
- [97] A. Park Williams, Edward R. Cook, Jason E. Smerdon, Benjamin I. Cook, John T. Abatzoglou, Kasey Bolles, Seung H. Baek, Andrew M. Badger, and Ben Livneh. Large contribution from anthropogenic warming to an emerging north american megadrought. *Science*, 368(6488):314–318, 2020.
- [98] Eric J.H. Wilson, Chioke B. Harris, Joseph J. Robertson, and John Agan. Evaluating energy efficiency potential in low-income households: A flexible and granular approach. *Energy Policy*, 129:710–737, 2019.
- [99] Yongkang Xue, Zavisa Janjic, Jimy Dudhia, Ratko Vasic, and Fernando De Sales. A review on regional dynamical downscaling in intraseasonal to seasonal simulation/prediction and major factors that affect downscaling ability. *Atmospheric Research*, 147–148:68–85, Oct 2014.
- [100] Seleshi G. Yalem, Michelle T.H. van Vliet, David Gernaat, Fulco Ludwig, Ariel Miara, Chan Park, Edward Byers, Enrica De Cian, Franziska Piontek, Gokul Iyer, Ioanna Mouratiadou, James Glynn, Mohamad Hejazi, Olivier Dessens, Pedro Rochedo, Robert Pietzcker, Roberto Schaeffer, Shinichiro Fujimori, Shouro Dasgupta, Silvana Mima, Silvia R.Santos da Silva, Vaibhav Chaturvedi, Robert Vautard, and Detlef P. van Vuuren. Impacts of climate change on energy systems in global and regional scenarios. *Nature Energy*, 5(10):794–802, 2020. Publisher: Nature Research.
- [101] Zhenzhong Zeng, Alan D. Ziegler, Timothy Searchinger, Long Yang, Anping Chen, Kunlu Ju, Shilong Piao, Laurent Z. X. Li, Philippe Ciais, Deliang Chen, Junguo Liu, Cesar Azorin-Molina, Adrian Chappell, David Medvigy, and Eric F. Wood. A reversal in global terrestrial stilling and its implications for wind energy production. *Nature Climate Change*, 9(1212):979–985, Dec 2019.
- [102] Patrick Zippenfenig. Open-meteo.com weather api, 2023.
- [103] Jian Zuo, Stephen Pullen, Jasmine Palmer, Helen Bennetts, Nicholas Chileshe, and Tony Ma. Impacts of heat waves and corresponding measures: a review. *Journal of Cleaner Production*, 92:1–12, Apr 2015.

## Appendix A

### Weird Exam Answers

**About appendices:** Each appendix follow the same page-numbering rules as a regular chapter; the first page of a (multi-page) appendix is not numbered. By the way, the following are supposedly authentic answers to English GCSE exams!

- (1) The Greeks were a highly sculptured people, and without them we wouldnt have history.  
The Greeks also had myths. A myth is a female moth.
- (2) Actually, Homer was not written by Homer but by another man of that name.
- (3) Socrates was a famous Greek teacher who went around giving people advice. They killed him. Socrates died from an overdose of wedlock. After his death, his career suffered a dramatic decline.
- (4) Julius Caesar extinguished himself on the battlefields of Gaul. The Ides of March murdered him because they thought he was going to be made king. Dying, he gasped out: Tee hee, Brutus.
- (5) Nero was a cruel tyranny who would torture his subjects by playing the fiddle to them.
- (6) In midevil times most people were alliterate. The greatest writer of the futile ages was Chaucer, who wrote many poems and verses and also wrote literature.
- (7) Another story was William Tell, who shot an arrow through an apple while standing on his sons head.

- (8) Writing at the same time as Shakespeare was Miguel Cervantes. He wrote Donkey Hote. The next great author was John Milton. Milton wrote Paradise Lost. Then his wife died and he wrote Paradise Regained.
- (9) During the Renaissance America began. Christopher Columbus was a great navigator who discovered America while cursing about the Atlantic. His ships were called the Nina, the Pinta, and the Santa Fe.
- (10) Gravity was invented by Issac Walton. It is chiefly noticeable in the autumn when the apples are falling off the trees.
- (11) Johann Bach wrote a great many musical compositions and had a large number of children. In between he practiced on an old spinster which he kept up in his attic. Bach died from 1750 to the present. Bach was the most famous composer in the world and so was Handel. Handel was half German half Italian and half English. He was very large.
- (12) Soon the Constitution of the United States was adopted to secure domestic hostility. Under the constitution the people enjoyed the right to keep bare arms.
- (13) The sun never set on the British Empire because the British Empire is In the East and the sun sets in the West.
- (14) Louis Pasteur discovered a cure for rabbis. Charles Darwin was a naturalist who wrote the Organ of the Species. Madman Curie discovered radio. And Karl Marx became one of the Marx brothers.

## Appendix B

### Ode to Spot

**(Data, Stardate 1403827)** (A one-page chapter — page must be numbered!) Throughout the ages, from Keats to Giorchamo, poets have composed “odes” to individuals who have had a profound effect upon their lives. In keeping with that tradition I have written my next poem . . . in honor of my cat. I call it . . . Ode . . . to Spot. (Shot of Geordi and Worf in audience, looking mystified at each other.)

Felus cattus, is your taxonomic nomenclature  
 an endothermic quadruped, carnivorous by nature?  
 Your visual, olfactory, and auditory senses  
 contribute to your hunting skills, and natural defenses.  
 I find myself intrigued by your sub-vocal oscillations,  
 a singular development of cat communications  
 that obviates your basic hedonistic predilection  
 for a rhythmic stroking of your fur to demonstrate affection.  
 A tail is quite essential for your acrobatic talents;  
 you would not be so agile if you lacked its counterbalance.  
 And when not being utilized to aid in locomotion,  
 It often serves to illustrate the state of your emotion.

(Commander Riker begins to applaud, until a glance from Counselor Troi brings him to a halt.)  
 Commander Riker, you have anticipated my denouement. However, the sentiment is appreciated.  
 I will continue.

O Spot, the complex levels of behavior you display  
 connote a fairly well-developed cognitive array.  
 And though you are not sentient, Spot, and do not comprehend  
 I nonetheless consider you a true and valued friend.